

Maintaining fairness across distribution shift: do we have viable solutions for real-world applications?

JESSICA SCHROUFF, Google Research, United Kingdom
NATALIE HARRIS, Google Research, United Kingdom
OLUWASANMI KOYEJO, Google Research, USA
IBRAHIM ALABDULMOHSIN, Google Research, Switzerland
EVA SCHNIDER*, University of Basel, Switzerland
KRISTA OPSAHL-ONG, Google, USA
ALEX BROWN, Google Research, United Kingdom
SUBHRAJIT ROY, Google Research, United Kingdom
DIANA MINCU, Google Research, United Kingdom
CHRISTINA CHEN, Google Research, USA
AWA DIENG, Google Research, Canada
YUAN LIU, Google Research, USA
VIVEK NATARAJAN, Google Research, USA
ALAN KARTHIKESALINGAM, Google Research, United Kingdom
KATHERINE HELLER, Google Research, USA
SILVIA CHIAPPA, DeepMind, United Kingdom
ALEXANDER D'AMOUR, Google Research, USA

Fairness and robustness are often considered as orthogonal dimensions when evaluating machine learning models. However, recent work has revealed interactions between fairness and robustness, showing that fairness properties are not necessarily maintained under distribution shift. In healthcare settings, this can result in e.g. a model that performs fairly according to a selected metric in “hospital A” showing unfairness when deployed in “hospital B”. While a nascent field has emerged to develop *provable fair and robust* models, it typically relies on strong assumptions about the shift, limiting its impact for real-world applications. In this work, we explore the settings in which recently proposed mitigation strategies are applicable by referring to a causal framing. Using examples of predictive models in dermatology and electronic health records, we show that real-world applications are complex and often invalidate the assumptions of such methods. Our work hence highlights technical, practical, and engineering gaps that prevent the development of *robustly fair* machine learning models for real-world applications. Finally, we discuss potential remedies at each step of the machine learning pipeline.

Additional Key Words and Phrases: Machine Learning, Fairness, Robustness, Healthcare

*Work performed while interning at Google Research

Authors' addresses: Jessica Schrouff, Google Research, London, United Kingdom, schrouff@google.com; Natalie Harris, Google Research, London, United Kingdom; Oluwasanmi Koyejo, Google Research, Mountain View, CA, USA; Ibrahim Alabdulmohsin, Google Research, Zurich, Switzerland; Eva Schneider, University of Basel, Basel, Switzerland; Krista Opsahl-Ong, Google, Mountain View, CA, USA; Alex Brown, Google Research, London, United Kingdom; Subhrajit Roy, Google Research, London, United Kingdom; Diana Mincu, Google Research, London, United Kingdom; Christina Chen, Google Research, Mountain View, CA, USA; Awa Dieng, Google Research, Montreal, Canada; Yuan Liu, Google Research, Mountain View, CA, USA; Vivek Natarajan, Google Research, Mountain View, CA, USA; Alan Karthikesalingam, Google Research, London, United Kingdom; Katherine Heller, Google Research, Mountain View, CA, USA; Silvia Chiappa, DeepMind, London, United Kingdom; Alexander D'Amour, Google Research, Cambridge, MA, USA.

1 INTRODUCTION

As progress is made to integrate machine learning (ML) systems in real-world applications, a concern is to reduce disparities between subsets of the population (e.g. based on age, sex, race) impacted by ML. The ML community is approaching this issue from different perspectives: an assortment of metrics to assess potential (un)fairness across subgroups as well as techniques for mitigating unfairness have been proposed (see [5, 16, 39, 42, 46, 73] for overviews).

Fairness metrics and mitigation techniques currently used in real-world applications are typically evaluated on a single learning task or data distribution (e.g. [3, 10, 52, 77, 89]). Recent work has however highlighted that fairness properties that are satisfied on the data used to develop a model might not always hold if the data distribution changes [30, 33]. In high-risk domains like healthcare, this can translate to ‘if a model satisfies fairness criteria when trained in “Hospital A”, it may not satisfy them when tested in “Hospital B”’. Fueled by this observation, a new field of research is emerging to understand the relationship between ML fairness and robustness to distribution shift (e.g. [2, 14, 61, 72, 87]) and to provide mitigation techniques for obtaining *robustly fair* ML models (e.g. [64, 65, 67, 88]).

Importantly, the success of robustly fair machine learning depends strongly on the nature of the distribution shifts that the system will encounter in practice. This point has been made elegantly in work that uses causal structure to provide fairness guarantees under distribution shift [64, 67]. However, these guarantees are only practical when distribution shifts satisfy rather strict assumptions on their causal structure, namely, that the shift only directly affect parts of the data generating process in isolation.

The key contribution of this work is to assess how realistic these assumptions are by examining plausible distribution shifts in two applications of machine learning in dermatology and clinical risk prediction. In these contexts, we use statistical tests to show that clinically plausible shifts directly affect many aspects of the data distribution simultaneously. We then demonstrate empirically that such compound shifts have practical impact on the transferability of fairness properties in these applications. Our results highlight fundamental limitations of purely algorithmic approaches to achieving robustly fair models in practice. Our hope is that this work will spark additional research into a broader set of remedies across the entire ML pipeline for applications where models are expected to behave fairly across a range of real-world settings.

Our contributions can be summarized as follows: (1) we contextualize a number of recent transferable fairness approaches into a causal framework; (2) we design statistical tests to characterize plausible distribution shifts in two medical applications; (3) we show that these shifts induce practically significant fairness violations in their respective applications; and (4) we summarize technical, practical and engineering gaps that prevent the development of robustly fair models and discuss potential remedies that span the ML pipeline.

2 SETTING AND FORMALIZATION

Let A, X, Y denote random variables, where A represents one or more sensitive attributes (such as age, gender, or race), $X \in \mathcal{R}^d$ a set of features, and Y a categorical or continuous outcome. We consider a classification or regression model $f : \text{dom}(X') \rightarrow \text{dom}(Y)$ that outputs a prediction $f(X')$ of Y based on $X' = A \cup X$ or $X' = X$, and are interested in studying the fairness properties of f when the distribution of the data on which f is deployed is different from the one in which f is trained/validated. More specifically, denoting with S a random variable representing a specific environment, such as e.g. a geographical area, a given hospital or a limited period in time, we assume a *source environment* ($S = 0$) and a *target environment* ($S = 1$), and consider how fairness properties generalize when f is trained/validated on a dataset of samples from the distribution $P(A, X, Y | S = 0)$ but deployed on samples from the distribution $P(A, X, Y | S = 1)$.

Fairness. Our work focuses on statistical group definitions of fairness [5]. In particular, we frame the discussion around demographic parity in which the model’s output is statistically independent of the sensitive attribute, i.e. $f(X') \perp\!\!\!\perp A$, and equalized odds in which the independence holds conditionally on the outcome, i.e. $f(X') \perp\!\!\!\perp A | Y$. In the experiments, these metrics are computed according to Supplement A.1 for binary tasks. We also compute the gap in subgroup accuracy, as this is amenable to multiclass tasks. For all fairness metrics, the lower, the better.

Causal framework. We formalize the interplay between fairness and distribution shift using causal Bayesian networks [50, 51, 66], which are directed acyclic graphs in which nodes represent random variables and links express causal relationships between them (see Supplement A.2 for an introduction). In a causal Bayesian network, a node X^i is a *cause* of node X^j if there exists a *causal path* $X^i \rightarrow \dots \rightarrow X^j$ from X^i to X^j such that intervening on X^i affects X^j , but not conversely. If the path is direct, i.e. has not intermediate nodes, then X^i is called a *direct cause* of X^j . $\text{pa}(X^i)$ denote the *parents* of X^i , namely the nodes with a link into X^i . We use causal Bayesian networks to express relationships between A, X, Y , and between these variables and the environment S , following the joint causal inference framework proposed in [43]. We then assess when the (conditional) distributions of A, X and/or Y are preserved across the environments and define a ‘robustly fair’ model as a model whose fairness properties are independent of S .

Distribution shift. We categorize distribution shifts into the following four categories:

- *Demographic shift:* a shift in the distribution of the demographics A of the population, $P(A | S = 0) \neq P(A | S = 1)$, that is due to the presence of a direct path $S \rightarrow A$ in the causal graph, i.e. to S being a direct cause of A . An example of such a shift is a different proportion of female patients in $S = 0$ and in $S = 1$.
- *Covariate shift:* a shift in the distribution of the features X , $P(X | \text{pa}(X), S = 0) \neq P(X | \text{pa}(X), S = 1)$, that is due to a direct path $S \rightarrow X$. A covariate shift can be induced e.g. by using different cameras or views to acquire an image in $S = 0$ and $S = 1$ (acquisition shift) [7].
- *Label shift:* a shift in the distribution of the outcome Y , $P(Y | \text{pa}(Y), S = 0) \neq P(Y | \text{pa}(Y), S = 1)$, that is due to a direct path $S \rightarrow Y$. A label shift can manifest itself via a different prevalence of a disease in $S = 0$ compared to $S = 1$ (prevalence shift), and/or different strategies to obtain labels, e.g. silver standard vs gold standard, in $S = 0$ and $S = 1$ (annotation shift) [7].
- *Compound shift:* a shift that is due to a combination of some of the three above shifts. Compound shifts are typical in real-world applications. For instance, it is common for healthcare ML models to be trained on one or multiple datasets, and then be deployed on datasets recorded in other locations [79, 86]. Another example is that of a new device on the market [24]. Such device might be available to a specific demographic population, which could potentially be more healthy. This device will also affect the resulting image. Hence introducing the device simultaneously affects A, X and Y . More examples of shifts observed in clinical settings are discussed in [24].

These definitions are independent of the causal graph considered. We define demographic, covariate and label shifts as mutually exclusive, e.g. the presence of a direct causal path between S and A prevents direct paths between S and Y or S and X , as any other combination would be referred to as a ‘compound’ shift. We note that when considering causal graphs of X, Y and S only, we recover the assumptions typically associated with covariate shift (i.e. $S \rightarrow X \rightarrow Y : P(Y | X, S = 0) = P(Y | X, S = 1)$) and label shift (i.e. $S \rightarrow Y \rightarrow X : P(X | Y, S = 0) = P(X | Y, S = 1)$).

3 RELATED WORK

Robustness to distribution shift: has been investigated from many different angles. Extensive reviews on the topic exist [22, 48, 75, 78], and generally distinguish between the type of information available about the shift. We consider the setting in which the shifts are known and the target distribution(s) (i.e. $P(A, X, Y | S = 1)$ or $P(A, X | S = 1)$) are

available at training time (we refer to this setting as *domain adaptation* [6], and as *causal domain adaptation* if shifts are expected on specific paths of a causal graph), and the setting in which no information is given about the shift (we refer to this setting as *domain generalization*). With regards to the nature of the shifts, the literature typically targets either covariate shift, i.e. (combinations of) demographic and covariate shifts according to our definitions, or label shift. The research on these shifts is imbalanced, with label shift being less studied [36]. The work of [36] proposes an approach to detect a label shift and correct it using unlabelled target data. More recently, [25] unified multiple techniques. None of the works cited above center on simultaneous label and covariate shifts, or consider their interaction with fairness. **Fairness and robustness:** Nevertheless, relations between robustness guarantees and individual and group fairness have been studied in [44, 81, 83, 84] and in [72] respectively. [2, 14, 87] have also investigated the relationship between fairness and distribution shift experimentally by studying how robustness mitigation strategies affect fairness metrics. Work explicitly investigating fairness properties under distribution shift can mostly be divided into methods that provide a priori *guarantees* or *bounds* (e.g. [61, 64, 67]) and methods that *adapt* to the new distribution (e.g. [12, 19, 30, 47, 65, 68, 88]). Schumann et al. [61] provide bounds on fairness transfer and suggest to add adversarial heads on both the in-source attribute A and the environment S . We cast this work into a causal framework in Section 4. Of particular relevance is the recent work of ‘feature selection’ [38] which considers a set $\{V\}$ of variables to include as inputs to the model such that $\{V\}$ d-separates Y from S , namely $Y \perp\!\!\!\perp S \mid \{V\}$. This condition alone does not provide fairness guarantees under distribution shift. Singh et al. [64] then add the condition that $\{V\} \perp\!\!\!\perp S \mid A$ for demographic parity or $\{V\} \perp\!\!\!\perp S \mid Y, A$ for equalized odds. While the proposed method can capture simultaneous shifts across different paths of the causal graph by referring to causal domain adaptation, it explicitly does not take label shift into account.

Another line of work considers adapting transfer learning and meta-learning algorithms to consider fairness constraints and therefore ensure generalization to new tasks also in terms of fairness [12, 47, 65, 88]. Specifically, Coston et al. [12] modify the standard approach to transfer learning under covariate shift by adding a constraint to the weight learning objective that enforces closeness between all pairs of protected groups. Slack et al. [65] introduce a technique to identify mean shifts that could lead to unfairness. They then propose meta-learning with a regularizer that imposes demographic parity or equalized odds to improve the transfer of fairness. The method requires a small set of labelled target data (K-shot learning) and multiple tasks, and comes with no guarantees. Work on fine-tuning and transfer learning [47] leverages task similarity to learn fair representations that provably generalize to unseen tasks, similarly requiring a small set of labelled target data and generating a model per environment.

We discuss the applicability of these works to compound shifts in real-world applications in Section 4, with a special interest for the work of Singh et al. [64] and Slack et al. [65].

4 TECHNICAL AND PRACTICAL LIMITATIONS

In this section, we review how various transferable fairness approaches that have been proposed in the literature interact with different causal structures of domain shift depicted in Figures 1 and 2. We assume the same sensitive attributes A in the source and target environments, and consider different relationships between the environment and other variables. As in [7, 72], we split the analysis into causal or anti-causal prediction tasks [60]. A prediction task is causal if the features X are causes of the outcome Y , and anti-causal if the outcome Y is a cause of the features X . Many risk prediction problems are causal, where risk factors may cause an adverse outcome, while many diagnostic problems are anti-causal, where the underlying disease may cause symptoms [7].

A takeaway from this review is that most methods are tailored to particular restricted shift structures, and their useful properties can break down under compound shifts.

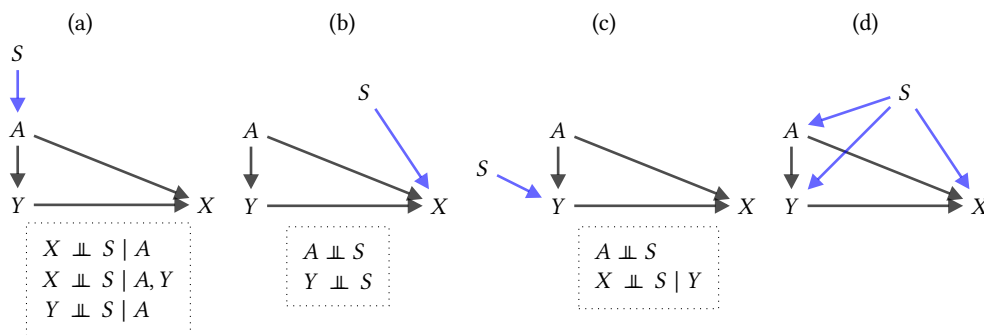


Fig. 1. Causal graphs under different distribution shifts when considering an anti-causal prediction task. (a) Demographic shift where the demographics A are directly affected by S . (b) Covariate shift where the X is directly affected by S . (c) Label shift where Y is directly affected by S . (d) Compound shift given by the combination of demographic, covariate, and label shifts.

4.1 Anti-causal prediction tasks

First, we consider anti-causal prediction tasks, in which the outcome Y is a direct cause of the features X , and that the sensitive attribute A is a direct cause of X and Y (the reality will likely be more complex and involve other variables in the paths (observed or not)). The assumption that A is a cause of X and Y is a reasonable approximation in healthcare settings: e.g. on average, skin images from men are more hairy than those of women, breasts are visible in chest x-rays, and comorbidities are different across sexes and age ranges. Sensitive attributes can also be related to the label, as prevalence can vary across subgroups (e.g. baldness is more prevalent in older patients) and some conditions might present differently across attributes (e.g. a heart attack in men vs women).

In this context, we consider strategies for learning robustly fair models under demographic, covariate, label and compound distribution shift scenarios represented in the causal graphs of Figure 1:

a) Demographic shift. In Figure 1(a), we consider a demographic shift through the direct path $S \rightarrow A$. In this case, the effects of S on Y and X are intercepted by A . Therefore, training a fair model based on X (either via imposing equalized odds [64] or counterfactual invariance with respect to A [72]) leads to a robustly fair model.

b) Covariate shift. In Figure 1(b), we consider a covariate shift through the direct path $S \rightarrow X$. In this case, there are multiple causal arrows into X that need to be addressed: $A \rightarrow X$ for fairness, and term $S \rightarrow X$ for robustness to distribution shift. In the case where some labeled target domain data is available, Schumann et al. [61] implement separate independence regularizers to address each path, and demonstrate its effectiveness in settings that match this causal structure. In the fully unlabeled domain adaptation case, the shift is harder to account for. For example, the set of features that satisfy the selection criteria of Singh et al. [64] would only include A , leading to a predictor that relies solely on demographics data (Supplement A.3).

c) Label shift. Lipton et al. [36] propose a technique to detect a label shift, as well as mitigate it through reweighting, requiring unlabelled target data. This technique can be used in addition to a fairness mitigation technique to lead to a robustly fair model.

d) Compound shift. Such a shift leads to multiple factors being affected by S , and current techniques would either be ineffective or degenerate to the trivial predictor. While Figure 1(d) represents the worst case scenario, even simpler combinations of shifts would lead to similar results in practice. For instance, adding a correlation between S and A to Figure 1(b) leads to a compound shift. In this specific case, mitigation might be possible by taking all intersections of A

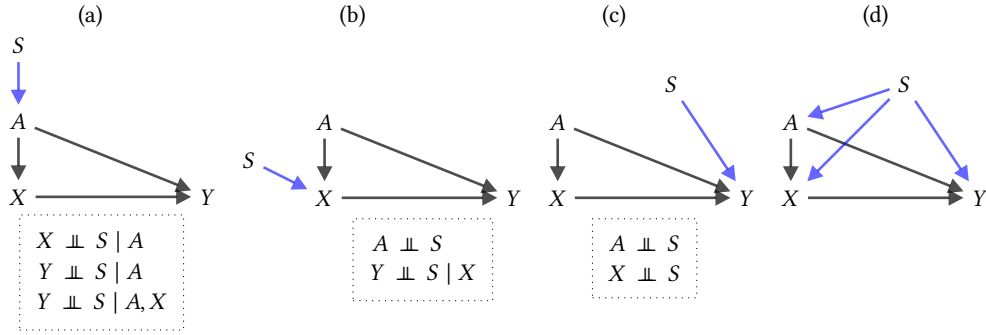


Fig. 2. Causal graphs under different distribution shifts when considering a causal prediction task. (a) Demographic shift, (b) Covariate Shift, (c) Label shift, and (d) Compound shift.

and S when using [61]. In practice, if the attribute or the shift have multiple discrete values, this will quickly become intractable, especially if distribution matching needs to be applied within each mini-batch. When considering feature selection, [64] would return an empty set for both equalized odds or demographic parity, leading to a trivial predictor. (Partial) mitigation might be obtained through the use of an adaptation technique as proposed in [47, 65].

4.2 Causal prediction tasks

We repeat the analysis above for the simplest causal prediction task in which X is a direct cause of Y , and assuming that A is a direct cause of X and Y . We then consider the following distribution shift scenarios represented in Figure 2:

a) Demographic shift. As in the anti-causal case, the relationship between X and Y is not affected by S if we impose invariance of Y on A . To this end, training a fair model based on the set $\{X, A\}$ would lead to a robustly fair model [64].

b) Covariate shift. In this setting, note that $(Y, A) \perp\!\!\!\perp S | X$. Thus, fairness and robustness to distribution shift guarantees can be obtained independently. This setting corresponds to the classic covariate shift scenario treated in much of the domain adaptation literature, where potential solutions are to match the distributions of X across environments by strategies such as reweighting [e.g. 62] or invariant representation learning [e.g. 6]. The advantage of such a techniques is that they only require unlabelled target data.

c) Label shift. While solutions are investigated for anti-causal prediction tasks, label shifts on causal prediction tasks are understudied and the absence of a direct path $S \rightarrow Y$ is often an assumption for mitigation techniques [64, 72]. To the best of our knowledge, there is no method proposing formal fairness guarantees under label shift in causal prediction tasks.

d) Compound shift. As for the anticausal case, a compound shift would lead to insufficient or trivial predictors.

5 ILLUSTRATION WITH REAL-WORLD HEALTHCARE APPLICATIONS

In this section, we illustrate that the shifts encountered in real-world applications are typically compound by performing a series of statistical tests to assess the causal structure of distribution shifts encountered in real-world applications. We focus on the healthcare domain and select an anti-causal prediction task in dermatology, and a causal prediction task in Electronic Health Records (EHR). Given a sample of labelled target data, we test for various invariances based on simplified causal graphs of the applications, highlighting that distribution shifts directly affect multiple aspects of

the data distribution simultaneously. In both the dermatology and EHR cases, we show that fairness properties do not transfer across these compound shifts.

5.1 Assessing the causal structure of a shift

For each variable X^d in the graph, we are assessing whether there is a direct effect of the environment S on X^d . This operation is often non-trivial when X^d has causal ancestors that could also be affected by the shift; in this case, the distribution of X^d would differ between environments, but there would be no direct effect of S on X^d . To isolate the direct effect of S , we derive the set of variables $\{V\}$ that block all indirect paths from S to X^d and compute weights that balance these background variable across environments. We then test the hypothesis that the reweighted distributions of X^d match across the environments S . Depending on the dimensionality of X^d , different strategies are used for the testing [54]. See Supplement A.4 for the details of our testing procedure.

Compared to the test proposed in Slack et al. [65], our strategy, while requiring a causal graph of the application, allows to estimate the joint causal inference framework [43] and hence to identify which mitigation strategies might be applicable. In addition, the test in [65] requires features to be semantic, and thus is not directly applicable in the context of computer vision.

5.2 Predicting skin conditions in dermatology

In this task, we are interested in predicting common skin conditions (26 conditions plus an additional ‘other’ category to capture the long tail), based on one or multiple images of the pathology of interest and additional metadata [37]. As is relatively common in healthcare settings, the model is trained on source data, and considered for application on target data that has been collected using different protocols in a different clinical environment. The data used as source is a subset of the data described in [37]. Briefly, it consists of de-identified retrospective adult cases from a teledermatology service serving 17 sites from 2 states in the United States. Each case contained 1-6 clinical photographs of the affected skin areas as well as patient demographic information and medical history (for a complete list, see Table S1 of [37]). We split the source data such that it comprises 12,024 cases for training, 1,925 for validation and hyper-parameter tuning and 1,924 for testing. The target data, unobserved at model development time, comes from skin cancer clinics in Australia and New Zealand and was partially labelled, leading to 21,661 cases used for model evaluation. We consider a second target dataset of 1,843 labelled teledermatology cases from Colombia in Supplement B.3¹.

Ethics approval: the images and metadata were de-identified according to Health Insurance Portability and Accountability Act (HIPAA) Safe Harbor prior to transfer to study investigators. The protocol was reviewed by [Anonymous] IRB, which determined that it was exempt from further review under 45 CFR 46.

5.2.1 A compound shift. We first show that the shift between the source and the target data affects all relationships in the causal graph. To this end, we draw a simplified causal graph of the dermatology task at hand, similar in spirit to the anti-causal prediction task discussed in Section 4, but with added metadata. In the source data, we can divide the metadata in multiple variables: demographics A , co-morbidities/medical history M and symptoms X_s . Each of these plays a different role in the causal graph (see Figure 3(a)), with the graph itself becoming more complex. We however note that we omit unobservable variables such as environmental factors that could affect the skin or co-morbidities and medical history that are not recorded in the data.

¹The dermatology data is not available to the public

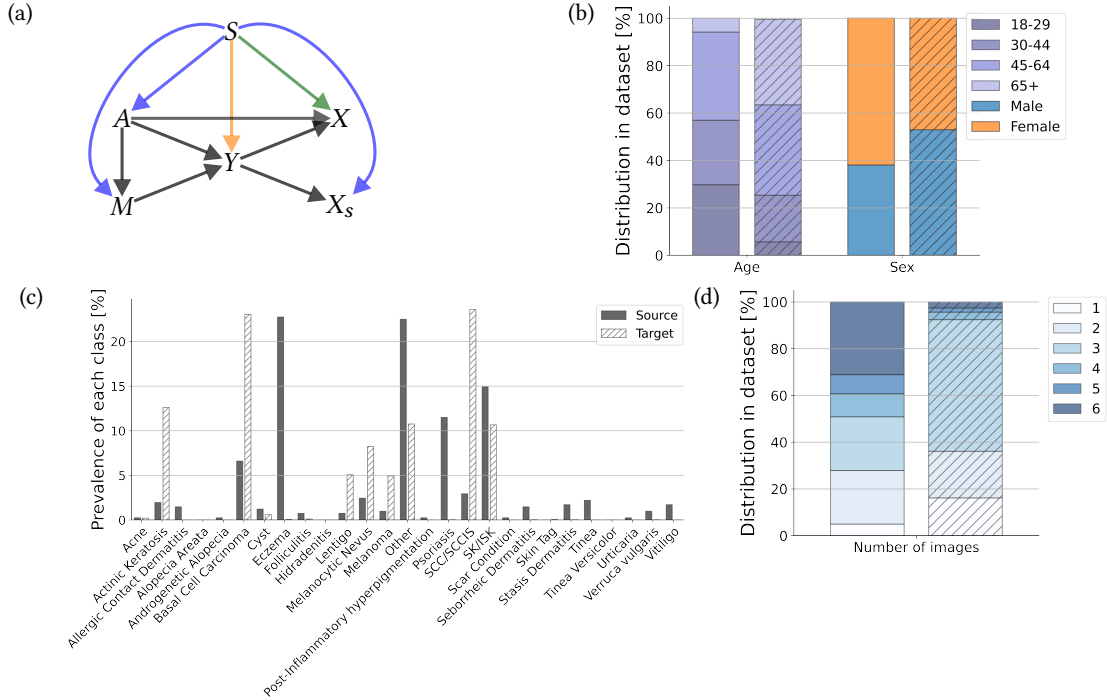


Fig. 3. A compound shift in dermatology. (a) Simplified causal structure of the application. A refers to demographic metadata, M to the patient’s medical history and comorbidities, Y to the skin condition as labelled by clinicians, X represents the set of pictures of the skin pathology and X_s represents other symptoms as shared by the patient (e.g. whether the lesion is ‘burning’ or ‘itchy’). In our setup, the environment S directly affects all variables in the graph. (b) Distribution in the source train and in the target dataset of the sensitive attributes, computed in terms of percentage of pre-defined subgroups. (c) Prevalence of each condition in cases where the patients are female and over 65 years of age. (d) Distribution of the number of images in cases labelled as ‘SK/ISK’ in older females. The distributions in the source data are represented on the left, and their corresponding distributions in the target data on their immediate right with a hashed pattern.

We first note that the metadata available in the source data is more comprehensive than the data available in the target data, with only age and sex² being common to both. These features have different distributions across the two datasets (see Figure 3(b)), with the population in the source data being typically younger (median age: 40 years old, 25% quantile: 27, 75% quantile: 54) than in the target data (median age: 58 years old, 25% quantile: 44, 75% quantile: 70). The source distribution also includes more female patients than the target data (62%, compared to 47%). Other demographics and its proxies (e.g. pregnancy status, ethnicity, skin type), as well as M and X_s are absent from the target data. We therefore see direct effects of S on M , X_s and A , and add these relationships to the causal graph (Figure 3a, in purple).

We then assess whether S directly affects the labels. By looking at the graph, we see that a shift on $P(A)$ could lead to a shift on the marginal $P(Y)$. However, conditioning on A and M could lead to an invariance of Y on S . As M is absent from the target data, we condition on A only. Using overlap weights to represent the conditioning [35], we obtain significant differences between $P(Y | A, S = 0)$ and $P(Y | A, S = 1)$ for 24 conditions ($p < 0.05$, Bonferroni corrected). Figure 3(c) illustrates the label shift in a specific age and sex subgroup (here females aged 65+, 409 cases in the source,

²Sex is mainly recorded by clinicians, with a small set of the source data containing self-reported sex.

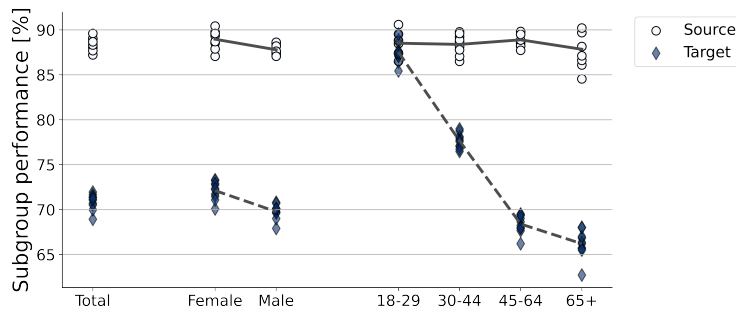


Fig. 4. Model performance in dermatology, as estimated via Top-3 accuracy (in %). The plot displays the total performance, as well as performance stratified by sex and by age on the source (circles with plain line) and target (diamonds with dashed line) data. Each marker represents one replicate of the model.

3,198 in the target data). We see that the source data includes more cases of ‘eczema’ and ‘psoriasis’ and that cancerous conditions such as ‘basal cell carcinoma’ and ‘melanoma’ are more prevalent in the target data. While this analysis is limited due to the absence of M and of sensitive attributes in the target data, our results suggest that the environment also directly affects the labels (indicated by the orange link in Figure 3(a)). We note that this analysis is limited to the distribution of labels and cannot assess differences in their quality: for instance, the labels for the source data were sourced from multiple clinicians, while some target labels were verified by biopsies. This is an added difference between the two environments (known as annotation shift, [7]) that only in-depth dataset knowledge can bring.

Finally, we consider whether the features of the images themselves (designated by X) are directly affected by S . If the environment does not directly affect the images, then $P(X | Y, A, S = 0) = P(X | Y, A, S = 1)$. However, our weighted t-tests suggest a significant difference between these two distributions ($p < 0.05$ corrected on 22 dimensions). Figure 3(d) illustrates this difference by computing the number of images per case in the group of older females considered above with cases labelled as ‘SK/ISK’ (source median: 3, $n = 61$, target median: 2, $n = 341$). This result suggests the existence of the direct path $S \rightarrow X$ and we add this relationship to the graph (green link in Figure 3(a)).

Based on these different analyses, we conclude that the environment is affecting all the nodes in our simplified causal graph, which contrasts with previous works investigating the transferability of fairness. Similar results are obtained for the second target dataset considered, although 17 conditions present invariances to S after controlling for demographics (see Supplement B.3).

5.2.2 Fairness metrics are affected by the environment. We train a deep learning model to predict skin conditions from the images X , age and sex. Our research model follows the overall approach described in [37, 57] with some minor architectural changes. We use the train and validation sets of the source data to train 10 replicates of the model from different random seeds. Each model is then evaluated based on its top-1 and top-3 accuracy across all conditions on the test set of the source data and on the target data. We assess fairness by estimating the difference in top-k model performance between subgroups. When multiple subgroups refer to the same sensitive attribute, we compute the maximum difference between any pair of subgroups.

Overall, our model performs in line with [37, 57] on the source data³, obtaining a top-3 accuracy of $88.52 \pm 0.68\%$. When stratifying per sex, the model performs slightly better for females ($88.95 \pm 0.93\%$) than for males ($87.78 \pm 0.52\%$).

³Notice that we are only using a subset of the data, and different splits, leading to an apparent decrease in performance (93% in [37] compared to 88% here).

We also observe a 1.05% maximum difference across age subgroups (based on binary comparisons), with the 65+ group under-performing ($87.84 \pm 1.70\%$). We however note that these numbers are close to one another, and that there is no significant difference when considering multiple training seeds. Therefore, not performing any fairness mitigation might seem like a reasonable option.

Nevertheless, the gaps between the groups increase when the environment changes (Figure 4), with the difference between females and males doubling (from 1.17 to 2.33%) and the maximum age gap reaching 21.32%. Similar results are obtained when considering top-1 accuracy (Supplement B.2.2). When considering conditions separately, the patterns can vary, but often differ between the source and the target data (Supplement B.2.3). We therefore observe that the fairness metrics are affected by the environment. These results are replicated for the other target dataset considered, leading to similar conclusions. Interestingly, considering only those 17 conditions displaying invariance to S leads to a noticeable reduction in fairness metric disparities between environments (Supplement B.3.2).

5.2.3 Current mitigation techniques for fairness violations under distribution shift are not applicable. As we observed, the shift is complex and does not satisfy the assumptions in [64], or the independence between A and S required for [61]. In this case, the meta-learning strategy proposed in [65] cannot be directly applied as this is a single multiclass problem which does not refer to multiple tasks. In the present case, we also notice that (fairness) mitigation strategies for multiclass applications are scarce (e.g. [17, 82]).

In addition, the features are pixels and non-semantic, meaning that feature selection techniques that directly test for invariances based on the features are not applicable [38, 64]. On the other hand, masking has been used previously to constrain the learning towards specific areas of the image [56, 63]. In this case, each training image is accompanied by a segmentation of the lesion. By ‘zooming in’ on the lesion, we hope that the model will more easily isolate the signal of interest compared to confounding factors, without discarding (too much) useful signal. While this technique has shown some promise with chest x-rays [74], it is impractical due to the additional requirement of a mask for all training images. In addition, it increases the ratio of signal of interest compared to undesirable signal, but does not exclude such signals. Therefore, in cases where the undesirable signal remains strong in the masked area, the technique comes with no guarantee.

5.3 Clinical risk prediction from Electronic Health Records

In this application, we predict the clinical outcomes of patients based on EHRs. EHRs record the time series of interactions between a patient and the clinical system (e.g. medication, labs, vitals, ...). In the context of EHR data, evidence has previously shown heterogeneity across centers [80]. However, important shifts can also be observed within a single system [45]. As an example, over half of hospitals in the US with intensive care units (ICUs) only have a single unit where all critically ill patients (medical, surgical, cardiac, ...) are admitted [1]. Risk scores, such as the Acute Physiology and Chronic Health Evaluation II (APACHE II) score are used to evaluate all critically ill patients, but do not perform equally across clinical subgroups, e.g. underperforming on patients with cardiac disease [53]. We illustrate this shift by considering a model developed on data from generalist ICUs and deployed on data from specialized ICUs. The dataset used in this study is the open access, de-identified Medical Information Mart for Intensive Care III (MIMIC-III) dataset [29]⁴, which consists of data from admissions to ICUs at the Beth Israel Deaconess Medical Center between 2001 and 2012. Based on clinical input, we consider the Medical ICU (MICU), Surgical ICU (SICU) and Trauma Surgical ICU (TSICU) to be generalist ICUs; whereas the Cardiac Surgery Recovery Unit (CSRU) and Coronary Care Unit (CCU) are

⁴The de-identified EHR data is available based on a user agreement at Physionet [26].

specialized ICUs. This split leads to 17,641 patients included in the source dataset and 10,442 patients in the target dataset after cohort selection. Our goal is to predict prolonged ICU stay (i.e. length of stay > 3 days, as in [52, 76]) using data from the first 24 hours of first ICU admission. Please see Supplement C.1 for additional information.

5.3.1 A compound shift. We frame this task by referring to the causal graph described in [64]. In their work, the authors used a restricted set of variables related to demographics A , comorbidities M , observed features X and the label Y . Similarly, we define the demographics A as age and self-reported sex, comorbidities M as previous medical history defined by ICD-9 codes [8, 18, 27, 34], observed features X as all labs and vitals, and Y as our prolonged length of stay label. Given that a more comprehensive feature set leads to better predictive performance [58], we use all 59,351 features at our disposal and add ‘treatments’ T (e.g. medications) to the graph (Figure 5(a)). In our graph, S represents the ICU unit type that a patient is admitted to and is therefore correlated with the ‘reason for the ICU visit’ R . We note that variables like labs and vitals might correlate with R but that the model does not have a direct access to R within the first 24 hours of admission for which the predictions are issued.

As performed in Section 5.2, we investigate potential (conditional) independencies between the environment and the different variables. We first estimate the distribution of age and sex in each dataset (Figure 5(b)). We observe that the population in the source is typically younger (median: 62 years old, 25% quantile: 49, 75% quantile: 76) than the population in the target (median: 68 years old, 25% quantile: 58, 75% quantile: 77, t-test: $p < 0.0001$). In addition, the proportion of males in the source and target differ (source: 50%, target: 65%). Therefore, $A \not\perp S$.

To assess comorbidities, we refer to Elixhauser and Vanwalraven scores for comorbidities [21, 71] and compute the scores on the source and target data [28]⁵. Figure 5(c) displays the distribution of comorbidities in a specific slice of the data (here older males, $n = 3,951$ in source and $n = 3,588$ in target). As expected, patients in the target data have a higher prevalence of comorbidities related to the peripheral vascular system than in the source data and $M \not\perp S | A$ for 8 comorbidities (weighted t-test: $p < 0.05$, Bonferroni corrected).

We repeat the analysis to assess the direct effect of S on the treatments ($P(T | A, M, S = 0) = P(T | A, M, S = 1) : p < 0.0001$), on the labs and vitals ($P(X | A, M, T, S = 0) = P(X | A, M, T, S = 1) : p < 0.05$) and on the label ($P(Y | A, M, T, S = 0) = P(Y | A, M, T, S = 1) : p < 0.05$) in Supplement C.2. Figure 5(d) displays the prevalence of prolonged length of stay for the specific subgroup of older males with a history of a solid tumor comorbidity and receiving vasopressors/inotropes ($n = 55$ in source and $n = 16$ in target). Our results suggest that the shift is compound, i.e. the ICU unit a patient is admitted to will directly affect all variables in our causal graph. We note that this conclusion is not surprising clinically, given that the environment S is correlated with the reason for their ICU admission R , and that this reason for admission (unobserved) is a main driver for all variables.

5.3.2 Fairness metrics are affected by the shift. As performed in [58, 69, 70], each patient’s medical history is converted to a time series of one-hour aggregates including the different structured data elements (medication, labs, vitals, ...) represented by numerical and binary variables. Based on the first 24 hourly aggregates, we predict the binary label for prolonged length of stay using a recurrent network architecture [69, 70]⁶. We then estimate model performance in terms of accuracy across patients and per sex and age subgroups. In addition to per-group metrics, we compute demographic parity and equalized odds.

Figure 6(a) displays model accuracy across subgroups on the source and target data. On the source data, the model performs to $78.6 \pm 0.7\%$ accuracy, with $\sim 1\%$ performance gap between sex groups (Female: $77.8 \pm 0.8\%$, Male: $79.2 \pm 0.5\%$),

⁵Code publicly available at <https://doi.org/10.5281/zenodo.821872>

⁶We take inspiration from the code made publicly by the authors of [70] and available at <https://github.com/google/ehr-predictions>

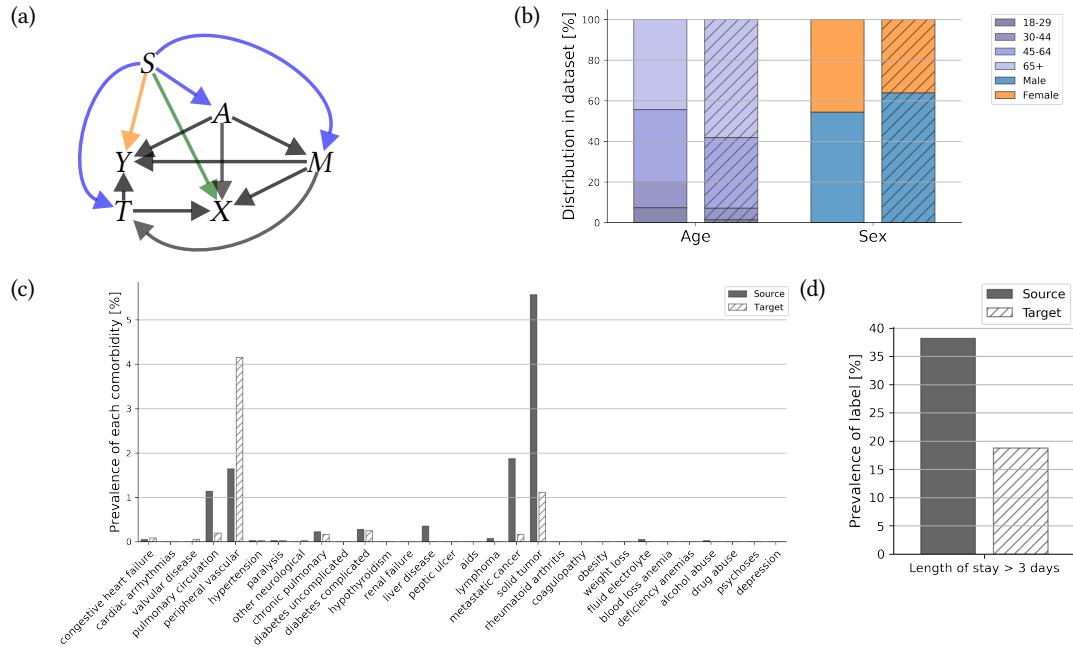


Fig. 5. A compound shift in EHR. (a) Causal graph for this application (see text for variable description). (b) Distribution in each dataset of the sensitive attributes, computed in terms of percentage of pre-defined subgroups. (c) Prevalence of comorbidities for male patients over 65 years of age. (d) Prevalence of the label for male patients over 65 with a solid tumor comorbidity and under vasopressors/inotropes. The distributions in the source data (train split) are represented on the left, and their corresponding distributions in the target data on their immediate right with a hashed pattern.

and a gap of 7.4% between age subgroups (18-29: $84.0 \pm 1.6\%$, 30-44: $82.8 \pm 0.9\%$, 45-64: $78.8 \pm 0.5\%$, 65+: $76.6 \pm 0.7\%$). Performance increases slightly between the two environments, with the model reaching $79.7 \pm 0.9\%$. The gap between sexes increases to 2.7% on the target data (Female: $78.0 \pm 0.6\%$, Male: $80.7 \pm 0.5\%$). For ages, the maximum gap remains similar (7% on average across seeds, 18-29: $82.5 \pm 0.9\%$, 30-44: $84.2 \pm 0.9\%$, 45-64: $83.2 \pm 0.6\%$, 65+: $77.2 \pm 0.6\%$).

In terms of fairness metrics, demographic parity is 0.002 ± 0.002 for sex on the source, and 0.016 ± 0.003 on the target. It is 0.05 ± 0.006 for age on the source, and 0.066 ± 0.010 on the target. For both attributes, we hence observe an increase in demographic parity between the source and the target. Equalized odds do not display a significant difference between the two environments, for age or sex. On the other hand, we observe significant differences in model accuracy for specific subgroups (e.g. 45-64 years old) between the two environments, suggesting that investigating the predictions for specific subgroups is needed, in addition to computing overall scores like demographic parity, equalized odds or maximum performance gaps.

5.3.3 Fairness properties after mitigation do not transfer. As the gap between age groups in the source is considerable, we perform post-processing of the predictions to enforce either demographic parity or equalized odds across age subgroups. We use the method in Alabdulmohsin and Lučić [4], fitting the debiasing model on the tune split of the source, and applying it to the test set of the source and to the target set.

Preprint – do not distribute.

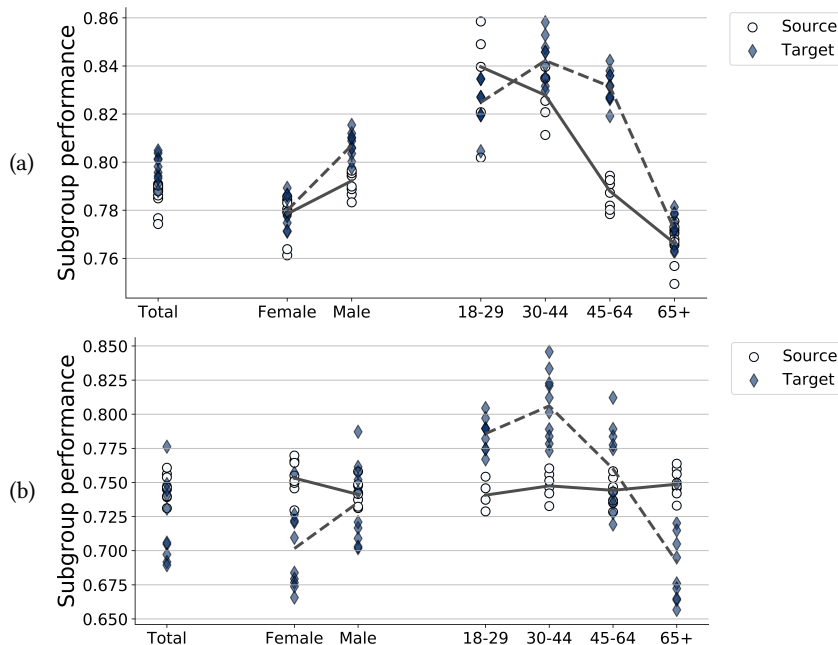


Fig. 6. Model performance in EHR, as estimated via accuracy. The plot displays the total performance, as well as performance stratified by sex and by age on the source (circles with plain line) and target (diamonds with dashed line) data. Each marker represents one replicate of the model. (a) Un-mitigated. (b) After mitigating for equalized odds across age groups on the source data.

This results in demographic parity to decrease to value 10^{-5} in the source, but to (slightly) increase to value 0.078 ± 0.025 in the target data. Similarly, equalized odds decrease to value 10^{-5} and the gap in model accuracy between groups is reduced from 7% to 0.8% (Figure 6(b)) in the source, but increases from 0.05 ± 0.008 to 0.16 ± 0.04 on the target data, and the gap between age groups increases to 11.4%.

We therefore observe that mitigating for either demographic parity or equalized odds on the source leads to no improvement, or even worsening of the fairness properties on the target. Noteworthy, the variance across seeds also increases on the target, which might highlight a manifestation of underspecification [15].

5.3.4 Current mitigation for fairness violations under distribution shift are not applicable. Singh et al. [64] clearly mention which shifts can be accounted for by their feature selection strategy: shifts that are mediated by A (i.e. $S \rightarrow A \rightarrow X^d$), or shifts that affect variables X correlated with the outcome Y . For the latter, affected variables are considered as ‘unstable’ and need to be removed from the input feature set. In the present case, the graph is more complex, as is the shift, and the covariate shift assumption is not valid (i.e. here $Y | A, M, T \not\perp S$). Therefore, the method would lead to an empty feature set. We also note that shifts affecting single variables in X are unlikely due to the presence of correlations among variables (e.g. labs sampled as part of ‘panels’ and not in isolation). In terms of experimentally-driven techniques, we observe the same limitation as for dermatology, whereby we only have a single task and the work of Slack et al. [65] is not directly applicable. Engineering-wise, it is also unclear how provable transfer techniques could apply to the recurrent, multidimensional, sparse problem that represents EHR modeling.

6 DISCUSSION

In this work, we formalized the interaction between population-level fairness and distribution shift using a causal framework. We used this formalization to discuss previous work and to investigate two healthcare applications. Our analysis highlighted the following *gaps* for the application of current unfairness mitigation methods in real-world settings:

- **Technical gap.** In the case of complex causal graph and shift, provable mitigation strategies for fairness violations under distribution shift have limited applicability in real-world settings. Therefore, currently available methods often lead to a solution with no guarantee or to a trivial predictor.
- **Practical gap.** Even experimentally-driven techniques [2, 61, 65] would need further work before they could be considered for the applications discussed in this work (e.g. single task, multivariate sparse time series).
- **Engineering gap.** Given a small sample of labelled target data, fine-tuned models that are provably fair [88] could be considered. These however come at the cost of maintaining one tuned model per environment, which is not sustainable for all real-world deployments of ML. Techniques relying on regularization (e.g. [61, 72]) also require that there be enough samples across the different subgroups to match the distributions of interest. Given that regularization is applied per batch, this necessitates batches that are of a minimal size (limiting for e.g. long time series in EHR) and diverse in terms of representation. This limitation can be compounded in low data settings, which are typical in healthcare.

Given that each task leads to different complexities in terms of causal graph, expected shifts, and fairness requirements, we can envisage remedies at every step of the ML pipeline [9]:

- (1) **Problem selection.** Consider focusing on tasks with lower anticipated harms or clinical/policy safeguards against ML unfairness.
- (2) **Data collection.** Consider early data collection from anticipated deployment environments in which distribution shifts are suspected. We indeed observed that statistical tests based on a (labelled) subset of the target data can provide evidence of how the environment affects the data and the task. In one case (second target dataset in dermatology), it allowed pinpointing the main drivers of the fairness gap between the source and the target to 10 conditions out of 27. In addition, Section 4 showed that if some invariances to the environment are observed, it is possible that an unlabelled or labelled sample from the target data could be used for mitigation or that feature selection [64] methods are applicable.
- (3) **Outcome definition.** Consider intermediate outcomes for which unfairness under distribution shift might be less consequential (e.g. image segmentation compared to diagnosis).
- (4) **Algorithm development.** Based on (2), some strategies can be used if their assumptions are satisfied. In addition, in the present work we used a causal framework. However, techniques that are not easily cast into this framework exist. For instance, manual feature engineering has been used to improve the robustness of EHR models to distribution shift [45]. While this work has not evaluated the fairness of the model in the source and target distributions, we believe that feature engineering might be a promising avenue to enforce specific inductive biases during learning while reducing the risks of distribution shifts. Compared to previous works on the topic (e.g. [7]), this would mean having an observable proxy for a latent variable Z that represents the patient’s health. As per [7], having access to Z would lead to the modelling task being invariant to some (not all) combinations of shift and attributes, hence producing more robustly fair models.

- (5) **Post-deployment.** Further safeguards may be envisaged to safely deploy ML systems, for example, commencing such deployments with a prospective observational (non-interventional) integration [24]. Transfer learning or retraining with site-specific updates might then be considered as necessary prior to interventional deployment. Finally, those deployments may be accompanied with robust post-market surveillance to continuously monitor not only the performance but also the fairness of the systems.

We note that, while our analysis focused on two healthcare applications, our observations are not limited to clinical settings and are likely relevant to many real-world applications.

Limitations and future work. In this work, we recast recent work on the transferability of fairness leveraging causal graphs, grouping prediction tasks as causal or anti-causal, inspired by [7, 36, 60, 72]. This grouping is, however, limiting since, as we observed, in real-world applications causal graphs often contain input features that are both the cause and the effect of the outcome (e.g. M and A are causes of Y in dermatology, while X and X_s are effects, and the set A, X is used for predicting Y). Similarly, the prediction task can be causal with silver standard labels (Y determined from images by dermatologists), but anti-causal with gold standard labels (Y obtained from biopsy), and label type can be mixed even within a single dataset due to sampling effects [7]. We also note that we ignored the temporal setting of EHR.

While our work covers different types of shift, and their interaction with sensitive attributes, future work should investigate further sources of shift and biases, such as sampling biases or missingness (especially relevant for EHR) [7, 87]. We refer the reader to Castro and Glocker [7] for a causal framing of shifts in the context of medical imaging, noting that the discussion does not include interactions with fairness or sensitive attributes.

By specifying causal graphs for each problem, we make assumptions about the relationships between variables. These assumptions might not represent the true underlying data generation process. For instance, in Section 4, we made assumptions about the relationship between the demographics, the covariates, and the labels. While most of our conclusions hold under slightly different relationships, assuming that A and X are correlated rather than directly related would mean that the technique in [64] leads to an empty set $\{V\}$ for a covariate shift on the causal graph in Figure 2(b). Therefore, this exercise might need to be replicated if different assumptions are considered. In addition, the effects of A could potentially be divided into ‘fair’ and ‘unfair’ effects, as proposed in [11, 41]. For real-world applications, further assumptions were made, e.g. considering the silver standard label in dermatology as a good approximation for the gold standard label (hence an anti-causal task) [7]. The value of these graphs is purely illustrative and should not be considered for medical applications without validation.

Furthermore, the data at hand usually represents a set of proxies for the underlying variables. Therefore, even if a shift seems to satisfy some invariance assumptions, there are no sharp guarantees [23]. This is especially true for demographic factors: features such as ethnicity, age or sex only approximate sensitive attributes. We are also limited by which factors are observed, across all environments. For instance, skin type is only available in the source data and in one target environment (Supplement B.3.3). In addition, the uneven distribution of the data across skin types leads to under-represented groups and comparisons/conclusions on such small numbers might be irrelevant and/or misleading. Future work will hence involve acquiring more demographic data to ensure that all sensitive attributes can be investigated with respect to fairness and its transferability.

In terms of metrics, we have focused mostly on demographic parity and equalized odds, due to their recent causal grounding [72]. Different metrics might, however, be affected differently, and it is possible that some metrics are more or less ‘sensitive’ to distribution shift. Similarly, different fairness mitigation strategies might be affected differently by distribution shift, although none provides guarantees under distribution shift. We also note that ‘fairness’ in the healthcare domain is an active discussion, and that equalized odds or demographic parity metrics do not consider

factors such as socio-determinants of health or health equity. As discussed in [52], considering human elicited metrics might be an avenue forward. Similarly, ‘fairness’ might change depending on the context [59] and different metrics might be relevant in different environments.

DECLARATIONS

Conflict of interest

The authors declare that they have no conflict of interest.

Funding

This work was funded by Google.

Data and method availability

The dermatology data is not available to the public. The de-identified EHR data is available based on a user agreement at Physionet [26]. The code for extracting Elixhauser and van Walren comorbidity scores from MIMIC-III is available at <https://doi.org/10.5281/zenodo.821872> [28]. We use publicly available code for EHR modelling at <https://github.com/google/ehr-predictions> [69, 70].

ACKNOWLEDGEMENTS

The authors would like to acknowledge and thank Lucas Dixon, Noah Broestl, Sara Mahdavi, Nenad Tomasev, Cameron Chen, Stephen Pfohl, Matt Kusner, Victor Veitch, Shannon Sequeira, Abhijit Guha Roy, Jan Freyberg, Aaron Loh, Martin Seneviratne, Patricia MacWilliams, Yun Liu, Christopher Semturs, Dale Webster, Greg Corrado and Marian Croak for their contributions to this effort.

REFERENCES

- [1] [n. d.]. Critical Care Statistics. <https://www.sccm.org/Communications/Critical-Care-Statistics>.
- [2] Robert Adragna, Elliot Creager, David Madras, and Richard Zemel. 2020. Fairness and Robustness in Invariant Learning: A Case Study in Toxicity Classification. (Nov. 2020). arXiv:2011.06485 [cs.LG]
- [3] Alekh Agarwal, Alina Beygelzimer, Miroslav Dudik, John Langford, and Hanna Wallach. 2018. A Reductions Approach to Fair Classification. In *Proceedings of the 35th International Conference on Machine Learning (Proceedings of Machine Learning Research, Vol. 80)*, Jennifer Dy and Andreas Krause (Eds.). PMLR, 60–69. <https://proceedings.mlr.press/v80/agarwal18a.html>
- [4] Ibrahim Alabdulmohsin and Mario Lučić. 2021. A Near-Optimal Recipe for Debiasing Trained Machine Learning Models. In *35th Conference on Neural Information Processing Systems (to appear)*. <https://arxiv.org/abs/2106.12887>
- [5] Solon Barocas, Moritz Hardt, and Arvind Narayanan. 2019. *Fairness and machine learning*. fairmlbook.org.
- [6] Shai Ben-David, John Blitzer, Koby Crammer, Alex Kulesza, Fernando Pereira, and Jennifer Wortman Vaughan. 2010. A theory of learning from different domains. *Mach. Learn.* 79, 1 (May 2010), 151–175.
- [7] Walker Ian Castro, Daniel C. and Ben Glocker. 2020. Causality matters in medical imaging. *Nature Communications* 11 (2020). Issue 1.
- [8] M E Charlson, P Pompei, K L Ales, and C R MacKenzie. 1987. A new method of classifying prognostic comorbidity in longitudinal studies: development and validation. *J. Chronic Dis.* 40, 5 (1987), 373–383.
- [9] Irene Y Chen, Emma Pierson, Sherri Rose, Shalmali Joshi, Kadija Ferryman, and Marzyeh Ghassemi. 2021. Ethical Machine Learning in Healthcare. *Annu Rev Biomed Data Sci* 4 (July 2021), 123–144.
- [10] Valeriia Cherepanova, Vedant Nanda, Micah Goldblum, John P Dickerson, and Tom Goldstein. 2021. Technical Challenges for Training Fair Neural Networks. (Feb. 2021). arXiv:2102.06764 [cs.LG]
- [11] Silvia Chiappa. 2019. Path-Specific Counterfactual Fairness. *AAAI* 33, 01 (July 2019), 7801–7808.
- [12] Amanda Coston, Karthikeyan Natesan Ramamurthy, Dennis Wei, Kush R. Varshney, Skyler Speakman, Zairah Mustahsan, and Supriyo Chakraborty. 2019. Fair Transfer Learning with Missing Protected Attributes. In *AAAI/ACM Conference on AI, Ethics, and Society*. 91–98.
- [13] Robert G. Cowell, A. Philip Dawid, Steffen Lauritzen, and David J. Spiegelhalter. 2007. *Probabilistic Networks and Expert Systems, Exact Computational Methods for Bayesian Networks*. Springer-Verlag.

Preprint – do not distribute.

- [14] Elliot Creager, Joern-Henrik Jacobsen, and Richard Zemel. 2021. Environment Inference for Invariant Learning. In *Proceedings of the 38th International Conference on Machine Learning (Proceedings of Machine Learning Research, Vol. 139)*, Marina Meila and Tong Zhang (Eds.). PMLR, 2189–2200.
- [15] Alexander D’Amour, Katherine Heller, Dan Moldovan, Ben Adlam, Babak Alipanahi, Alex Beutel, Christina Chen, Jonathan Deaton, Jacob Eisenstein, Matthew D Hoffman, Farhad Hormozdiari, Neil Houlsby, Shaobo Hou, Ghassen Jerfel, Alan Karthikesalingam, Mario Lucic, Yian Ma, Cory McLean, Diana Mincu, Akinori Mitani, Andrea Montanari, Zachary Nado, Vivek Natarajan, Christopher Nielson, Thomas F Osborne, Rajiv Raman, Kim Ramasamy, Rory Sayres, Jessica Schrouff, Martin Seneviratne, Shannon Sequeira, Harini Suresh, Victor Veitch, Max Vladymyrov, Xuezhong Wang, Kellie Webster, Steve Yadlowsky, Taedong Yun, Xiaohua Zhai, and D Sculley. 2020. Underspecification Presents Challenges for Credibility in Modern Machine Learning. (Nov. 2020). arXiv:2011.03395 [cs.LG]
- [16] E. Del Barrio, P. Gordaliza, and J.-M. Loubes. 2020. Review of Mathematical Frameworks for Fairness in Machine Learning. (2020). arXiv:2005.13755
- [17] Christophe Denis, Romuald Elie, Mohamed Hebiri, and François Hu. 2021. Fairness guarantee in multi-class classification. (Sept. 2021). arXiv:2109.13642 [math.ST]
- [18] R A Deyo, D C Cherklin, and M A Ciol. 1992. Adapting a clinical comorbidity index for use with ICD-9-CM administrative databases. *J. Clin. Epidemiol.* 45, 6 (June 1992), 613–619.
- [19] Wei Du and Xintao Wu. 2021. Fair and Robust Classification Under Sample Selection Bias. In *ACM International Conference on Information & Knowledge Management*. 2999–3003.
- [20] Cynthia Dwork, Moritz Hardt, Toniann Pitassi, Omer Reingold, and Richard Zemel. 2012. Fairness through awareness. In *Innovations in Theoretical Computer Science*.
- [21] A Elixhauser, C Steiner, D R Harris, and R M Coffey. 1998. Comorbidity measures for use with administrative data. *Med. Care* 36, 1 (Jan. 1998), 8–27.
- [22] Abolfazl Farahani, Sahar Voghoei, Khaled Rasheed, and Hamid R Arabnia. 2020. A Brief Review of Domain Adaptation. (Oct. 2020). arXiv:2010.03978 [cs.LG]
- [23] Noam Finkelstein, Roy Adams, Suchi Saria, and Ilya Shpitser. 2021. Partial Identifiability in Discrete Data With Measurement Error. In *Proceedings of 37th Conference on Uncertainty in Artificial Intelligence*.
- [24] Samuel G Finlayson, Adarsh Subbaswamy, Karandeep Singh, John Bowers, Annabel Kupke, Jonathan Zittrain, Isaac S Kohane, and Suchi Saria. 2021. The Clinician and Dataset Shift in Artificial Intelligence. *N. Engl. J. Med.* 385, 3 (July 2021), 283–286.
- [25] Saurabh Garg, Yifan Wu, Sivaraman Balakrishnan, and Zachary Lipton. 2020. A Unified View of Label Shift Estimation. In *Advances in Neural Information Processing Systems*, H Larochelle, M Ranzato, R Hadsell, M F Balcan, and H Lin (Eds.), Vol. 33. Curran Associates, Inc., 3290–3300.
- [26] A L Goldberger, L A Amaral, L Glass, J M Hausdorff, P C Ivanov, R G Mark, J E Mietus, G B Moody, C K Peng, and H E Stanley. 2000. PhysioBank, PhysioToolkit, and PhysioNet: components of a new research resource for complex physiologic signals. *Circulation* 101, 23 (June 2000), E215–20.
- [27] Patricia Halfon, Yves Eggli, Guy van Melle, Julia Chevalier, Jean Blaise Wasserfallen, and Bernard Burnand. 2002. Measuring potentially avoidable hospital readmissions. *J. Clin. Epidemiol.* 55, 6 (June 2002), 573–587.
- [28] Alistair Ew Johnson, David J Stone, Leo A Celi, and Tom J Pollard. 2018. The MIMIC Code Repository: enabling reproducibility in critical care research. *J. Am. Med. Inform. Assoc.* 25, 1 (Jan. 2018), 32–39.
- [29] Alistair E W Johnson, Tom J Pollard, Lu Shen, Li-Wei H Lehman, Mengling Feng, Mohammad Ghassemi, Benjamin Moody, Peter Szolovits, Leo Anthony Celi, and Roger G Mark. 2016. MIMIC-III, a freely accessible critical care database. *Sci Data* 3 (May 2016), 160035.
- [30] Nathan Kallus and Angela Zhou. 2018. Residual Unfairness in Fair Machine Learning from Prejudiced Data. In *International Conference on Machine Learning*. 2439–2448.
- [31] Alexander Kolesnikov, Lucas Beyer, Xiaohua Zhai, Joan Puigcerver, Jessica Yung, Sylvain Gelly, and Neil Houlsby. 2020. Big Transfer (BiT): General Visual Representation Learning. In *ECCV*.
- [32] Daphne Koller and Nir Friedman. 2009. *Probabilistic Graphical Models: Principles and Techniques*. MIT Press.
- [33] Chao Lan and Jun Huan. 2017. Discriminatory Transfer. (July 2017). arXiv:1707.00780 [cs.CY]
- [34] Bing Li, Dewey Evans, Peter Faris, Stafford Dean, and Hude Quan. 2008. Risk adjustment performance of Charlson and Elixhauser comorbidities in ICD-9 and ICD-10 administrative databases. *BMC Health Serv. Res.* 8 (Jan. 2008), 12.
- [35] Fan Li, Laine E Thomas, and Fan Li. 2019. Addressing Extreme Propensity Scores via the Overlap Weights. *Am. J. Epidemiol.* 188, 1 (Jan. 2019), 250–257.
- [36] Zachary Lipton, Yu-Xiang Wang, and Alexander Smola. 2018. Detecting and Correcting for Label Shift with Black Box Predictors. In *Proceedings of the 35th International Conference on Machine Learning (Proceedings of Machine Learning Research, Vol. 80)*, Jennifer Dy and Andreas Krause (Eds.). PMLR, 3122–3130.
- [37] Yuan Liu, Ayush Jain, Clara Eng, David H Way, Kang Lee, Peggy Bui, Kimberly Kanada, Guilherme de Oliveira Marinho, Jessica Gallegos, Sara Gabriele, Vishakha Gupta, Nalini Singh, Vivek Natarajan, Rainer Hofmann-Wellenhof, Greg S Corrado, Lily H Peng, Dale R Webster, Dennis Ai, Susan J Huang, Yun Liu, R Carter Dunn, and David Coz. 2020. A deep learning system for differential diagnosis of skin diseases. *Nat. Med.* 26, 6 (June 2020), 900–908.
- [38] Sara Magliacane, Thijs van Ommen, Tom Claassen, Stephan Bongers, Philip Versteeg, and Joris M Mooij. 2018. Domain Adaptation by Using Causal Inference to Predict Invariant Conditional Distributions. In *Advances in Neural Information Processing Systems*, S Bengio, H Wallach, H Larochelle, K Grauman, N Cesa-Bianchi, and R Garnett (Eds.), Vol. 31. Curran Associates, Inc.
- [39] Karima Makhlof, Sami Zhioua, and Catuscia Palamidessi. 2020. Survey on Causal-based Machine Learning Fairness Notions. arXiv:2010.09553

- [40] Ninareh Mehrabi, Fred Morstatter, Nripsuta Saxena, Kristina Lerman, and Aram Galstyan. 2019. A survey on bias and fairness in machine learning. *arXiv preprint arXiv:1908.09635* (2019).
- [41] Vishwali Mhasawade, Nabeel Abdur Rehman, and Rumi Chunara. 2020. Population-aware hierarchical bayesian domain adaptation via multi-component invariant learning. In *Proceedings of the ACM Conference on Health, Inference, and Learning* (Toronto, Ontario, Canada) (CHIL '20). Association for Computing Machinery, New York, NY, USA, 182–192.
- [42] Shira Mitchell, Eric Potash, Solon Barocas, Alexander D'Amour, and Kristian Lum. 2018. Prediction-based decisions and fairness: A catalogue of choices, assumptions, and definitions. *arXiv:1811.07867*
- [43] Joris M Mooij, Sara Magliacane, and Tom Claassen. 2020. Joint Causal Inference from Multiple Contexts. *J. Mach. Learn. Res.* 21, 99 (2020), 1–108.
- [44] Vedant Nanda, Samuel Dooley, Sahil Singla, Soheil Feizi, and John P Dickerson. 2021. Fairness Through Robustness: Investigating Robustness Disparity in Deep Learning. In *Proceedings of the 2021 ACM Conference on Fairness, Accountability, and Transparency* (Virtual Event, Canada) (FAccT '21). Association for Computing Machinery, New York, NY, USA, 466–477.
- [45] Bret Nestor, Matthew B A McDermott, Willie Boag, Gabriela Berner, Tristan Naumann, Michael C Hughes, Anna Goldenberg, and Marzyeh Ghassemi. 2019. Feature Robustness in Non-stationary Health Records: Caveats to Deployable Model Performance in Common Clinical Machine Learning Tasks. In *Proceedings of the 4th Machine Learning for Healthcare Conference (Proceedings of Machine Learning Research, Vol. 106)*, Finale Doshi-Velez, Jim Fackler, Ken Jung, David Kale, Rajesh Ranganath, Byron Wallace, and Jenna Wiens (Eds.). PMLR, Ann Arbor, Michigan, 381–405.
- [46] Luca Oneto and Silvia Chiappa. 2020. Fairness in Machine Learning. In *Recent Trends in Learning From Data. Studies in Computational Intelligence*, L. Oneto, N. Navarin, A. Sperduti, and D. Anguita (Eds.), Vol. 896. Springer, Cham.
- [47] Luca Oneto, Michele Donini, A. Maurer, and Massimiliano Pontil. 2019. Learning Fair and Transferable Representations. *arXiv:1906.10673*
- [48] Sinno Jialin Pan and Qiang Yang. 2010. A Survey on Transfer Learning. *IEEE Trans. Knowl. Data Eng.* 22, 10 (Oct. 2010), 1345–1359.
- [49] Judea Pearl. 1988. *Probabilistic Reasoning in Intelligent Systems: Networks of Plausible Inference*. Morgan Kaufmann Publishers Inc.
- [50] Judea Pearl. 2000. *Causality: Models, Reasoning, and Inference*. Cambridge University Press.
- [51] Judea Pearl, M. Glymour, and Nicholas P. Jewell. 2016. *Causal Inference in Statistics: A Primer*. Wiley.
- [52] Stephen R Pfohl, Agata Foryciarz, and Nigam H Shah. 2021. An empirical characterization of fair machine learning for clinical risk prediction. *J. Biomed. Inform.* 113 (Jan. 2021), 103621.
- [53] G L Pierpont and C M Parenti. 1999. Physician risk assessment and APACHE scores in cardiac care units. *Clin. Cardiol.* 22, 5 (May 1999), 366–368.
- [54] Stephan Rabanser, Stephan Günnemann, and Zachary C Lipton. 2019. Failing Loudly: An Empirical Study of Methods for Detecting Dataset Shift. In *33rd Conference on Neural Information Processing Systems* (Vancouver, Canada).
- [55] Alvin Rajkomar, Eyal Oren, Kai Chen, Andrew M Dai, Nissán Hajaj, Michaela Hardt, Peter J Liu, Xiaobing Liu, Jake Marcus, Mimi Sun, Patrik Sundberg, Hector Yee, Kun Zhang, Yi Zhang, Gerardo Flores, Gavin E Duggan, Jamie Irvine, Quoc Le, Kurt Litsch, Alexander Mossin, Justin Tansuwan, De Wang, James Wexler, Jimbo Wilson, Dana Ludwig, Samuel L Volchenboum, Katherine Chou, Michael Pearson, Srinivasan Madabushi, Nigam H Shah, Atul J Butte, Michael D Howell, Claire Cui, Greg S Corrado, and Jeffrey Dean. 2018. Scalable and accurate deep learning with electronic health records. *NPJ Digit Med* 1 (May 2018), 18.
- [56] Andrew Slavin Ross, Michael C Hughes, and Finale Doshi-Velez. 2017. Right for the right reasons: Training differentiable models by constraining their explanations. In *Proceedings of the Twenty-Sixth International Joint Conference on Artificial Intelligence* (Melbourne, Australia). International Joint Conferences on Artificial Intelligence Organization, California, 2662–2670.
- [57] Abhijit Guha Roy, Jie Ren, Shekoofeh Azizi, Aaron Loh, Vivek Natarajan, Basil Mustafa, Nick Pawlowski, Jan Freyberg, Yuan Liu, Zach Beaver, Nam Vo, Peggy Bui, Samantha Winter, Patricia MacWilliams, Greg S Corrado, Umesh Telang, Yun Liu, Taylan Cemgil, Alan Karthikesalingam, Balaji Lakshminarayanan, and Jim Winkens. 2021. Does Your Dermatology Classifier Know What It Doesn't Know? Detecting the Long-Tail of Unseen Conditions. (April 2021). *arXiv:2104.03829* [cs.CV]
- [58] Subhrajit Roy, Diana Mincu, Eric Loreaux, Anne Mottram, Ivan Protsyuk, Natalie Harris, Yuan Xue, Jessica Schrouff, Hugh Montgomery, Alistair Connell, Nenad Tomasev, Alan Karthikesalingam, and Martin Seneviratne. 2021. Multitask prediction of organ dysfunction in the intensive care unit using sequential subnetwork routing. *J. Am. Med. Inform. Assoc.* (June 2021).
- [59] Nithya Sambasivan, Erin Arnesen, Ben Hutchinson, Tulsee Doshi, and Vinodkumar Prabhakaran. 2021. Re-imagining Algorithmic Fairness in India and Beyond. (Jan. 2021). *arXiv:2101.09995* [cs.CY]
- [60] Bernhard Schölkopf, Dominik Janzing, Jonas Peters, Eleni Sgouritsa, Kun Zhang, and Joris Mooij. 2012. On Causal and Anticausal Learning. In *International Conference on Machine Learning*. 459–466.
- [61] Candice Schumann, Xuezhong Wang, Alex Beutel, Jilin Chen, Hai Qian, and Ed H Chi. 2019. Transfer of Machine Learning Fairness across Domains. (June 2019). *arXiv:1906.09688* [cs.LG]
- [62] Hidetoshi Shimodaira. 2000. Improving predictive inference under covariate shift by weighting the log-likelihood function. *Journal of statistical planning and inference* 90, 2 (2000), 227–244.
- [63] Becks Simpson, Francis Dutil, Yoshua Bengio, and Joseph Paul Cohen. 2019. GradMask: Reduce Overfitting by Regularizing Saliency. (April 2019). *arXiv:1904.07478* [cs.CV]
- [64] Harvineet Singh, Rina Singh, Vishwali Mhasawade, and Rumi Chunara. 2021. Fairness Violations and Mitigation under Covariate Shift. In *Proceedings of the 2021 ACM Conference on Fairness, Accountability, and Transparency*. Association for Computing Machinery, New York, NY, USA, 3–13.
- [65] Dylan Slack, Sorelle A Friedler, and Emile Givental. 2020. Fairness warnings and fair-MAML: learning fairly with minimal data. In *Proceedings of the 2020 Conference on Fairness, Accountability, and Transparency* (Barcelona, Spain) (FAT* '20). Association for Computing Machinery, New York, NY,

- USA, 200–209.
- [66] Peter Spirtes, Clark Glymour, and Richard Scheines. 2000. *Causation, Prediction, and Search*. MIT Press.
- [67] Adarsh Subbaswamy, Roy Adams, and Suchi Saria. 2020. Evaluating Model Robustness and Stability to Dataset Shift. (Oct. 2020). arXiv:2010.15100 [cs.LG]
- [68] Bahar Taskesen, Viet Anh Nguyen, Daniel Kuhn, and José H. Blanchet. 2020. A Distributionally Robust Approach to Fair Classification. arXiv:2007.09530
- [69] Nenad Tomašev, Xavier Glorot, Jack W Rae, Michal Zielinski, Harry Askham, Andre Saraiva, Anne Mottram, Clemens Meyer, Suman Ravuri, Ivan Protsyuk, Alistair Connell, Cian O Hughes, Alan Karthikesalingam, Julien Cornebise, Hugh Montgomery, Geraint Rees, Chris Laing, Clifton R Baker, Kelly Peterson, Ruth Reeves, Demis Hassabis, Dominic King, Mustafa Suleyman, Trevor Back, Christopher Nielson, Joseph R Ledsam, and Shakir Mohamed. 2019. A clinically applicable approach to continuous prediction of future acute kidney injury. *Nature* 572, 7767 (Aug. 2019), 116–119.
- [70] Nenad Tomašev, Natalie Harris, Sebastien Baur, Anne Mottram, Xavier Glorot, Jack W Rae, Michal Zielinski, Harry Askham, Andre Saraiva, Valerio Magliulo, Clemens Meyer, Suman Ravuri, Ivan Protsyuk, Alistair Connell, Cian O Hughes, Alan Karthikesalingam, Julien Cornebise, Hugh Montgomery, Geraint Rees, Chris Laing, Clifton R Baker, Thomas F Osborne, Ruth Reeves, Demis Hassabis, Dominic King, Mustafa Suleyman, Trevor Back, Christopher Nielson, Martin G Seneviratne, Joseph R Ledsam, and Shakir Mohamed. 2021. Use of deep learning to develop continuous-risk models for adverse event prediction from electronic health records. *Nat. Protoc.* 16, 6 (June 2021), 2765–2787.
- [71] Carl van Walraven, Peter C Austin, Alison Jennings, Hude Quan, and Alan J Forster. 2009. A modification of the Elixhauser comorbidity measures into a point system for hospital death using administrative data. *Med. Care* 47, 6 (June 2009), 626–633.
- [72] Victor Veitch, Alexander D’Amour, Steve Yadlowsky, and Jacob Eisenstein. 2021. Counterfactual Invariance to Spurious Correlations: Why and How to Pass Stress Tests. (May 2021). arXiv:2106.00545 [cs.LG]
- [73] Sahil Verma and Julia Rubin. 2018. Fairness definitions explained. In *IEEE/ACM International Workshop on Software Fairness*.
- [74] Joseph D Viviano, Becks Simpson, Francis Dutil, Yoshua Bengio, and Joseph Paul Cohen. 2019. Saliency is a possible red herring when diagnosing poor generalization. (Oct. 2019). arXiv:1910.00199 [cs.CV]
- [75] Jindong Wang, Cuiling Lan, Chang Liu, Yidong Ouyang, Wenjun Zeng, and Tao Qin. 2021. Generalizing to Unseen Domains: A Survey on Domain Generalization. (March 2021). arXiv:2103.03097 [cs.LG]
- [76] Shirly Wang, Matthew B A McDermott, Geeticka Chauhan, Michael C Hughes, Tristan Naumann, and Marzyeh Ghassemi. 2019. MIMIC-Extract: A Data Extraction, Preprocessing, and Representation Pipeline for MIMIC-III. (July 2019). arXiv:1907.08322 [cs.LG]
- [77] Zeyu Wang, Klint Qinami, Ioannis Christos Karakozis, Kyle Genova, Prem Nair, Kenji Hata, and Olga Russakovsky. 2020. Towards Fairness in Visual Recognition: Effective Strategies for Bias Mitigation. In *2020 IEEE/CVF Conference on Computer Vision and Pattern Recognition (CVPR)*. 8916–8925.
- [78] Karl Weiss, Taghi M Khoshgofaar, and Dingding Wang. 2016. A survey of transfer learning. *Journal of Big Data* 3, 1 (May 2016), 1–40.
- [79] Jenna Wiens, John Guttag, and Eric Horvitz. 2014. A study in transfer learning: leveraging data from multiple hospitals to enhance hospital-specific predictions. *J. Am. Med. Inform. Assoc.* 21, 4 (July 2014), 699–706.
- [80] F Perry Wilson, Melissa Martin, Yu Yamamoto, Caitlin Partridge, Erica Moreira, Tanima Arora, Aditya Biswas, Harold Feldman, Amit X Garg, Jason H Greenberg, Monique Hinchcliff, Stephen Latham, Fan Li, Haiqun Lin, Sherry G Mansour, Dennis G Moledina, Paul M Palevsky, Chirag R Parikh, Michael Simonov, Jeffrey Testani, and Ugochukwu Ugwuowo. 2021. Electronic health record alerts for acute kidney injury: multicenter, randomized clinical trial. *BMJ* 372 (Jan. 2021), m4786.
- [81] Han Xu, Xiaorui Liu, Yaxin Li, Anil Jain, and Jiliang Tang. 2021. To be Robust or to be Fair: Towards Fairness in Adversarial Training. In *Proceedings of the 38th International Conference on Machine Learning (Proceedings of Machine Learning Research, Vol. 139)*, Marina Meila and Tong Zhang (Eds.). PMLR, 11492–11501.
- [82] Forest Yang, Moustapha Cisse, and Sanmi Koyejo. 2020. Fairness with Overlapping Groups. (June 2020). arXiv:2006.13485 [cs.LG]
- [83] Samuel Yeom and Matt Fredrikson. 2020. Individual fairness revisited: Transferring techniques from adversarial robustness. In *Proceedings of the Twenty-Ninth International Joint Conference on Artificial Intelligence (Yokohama, Japan)*. International Joint Conferences on Artificial Intelligence Organization, California.
- [84] Mikhail Yurochkin, Amanda Bower, and Yuekai Sun. 2019. Training individually fair ML models with Sensitive Subspace Robustness. (June 2019). arXiv:1907.00020 [stat.ML]
- [85] Muhammad Bilal Zafar, Isabel Valera, Manuel Gomez Rodriguez, and Krishna P Gummadi. 2017. Fairness beyond disparate treatment & disparate impact: Learning classification without disparate mistreatment. In *International Conference on World Wide Web*.
- [86] John R Zech, Marcus A Badgeley, Manway Liu, Anthony B Costa, Joseph J Titano, and Eric Karl Oermann. 2018. Variable generalization performance of a deep learning model to detect pneumonia in chest radiographs: A cross-sectional study. *PLoS Med.* 15, 11 (Nov. 2018), e1002683.
- [87] Haoran Zhang, Natalie Dullerud, Laleh Seyyed-Kalantari, Quaid Morris, Shalmali Joshi, and Marzyeh Ghassemi. 2021. An empirical framework for domain generalization in clinical settings. In *Proceedings of the Conference on Health, Inference, and Learning (Virtual Event, USA) (CHIL ’21)*. Association for Computing Machinery, New York, NY, USA, 279–290.
- [88] Chen Zhao, Changbin Li, Jincheng Li, and Feng Chen. 2020. Fair Meta-Learning For Few-Shot Classification. In *IEEE International Conference on Knowledge Graph*. 275–282.
- [89] Jieyu Zhao, Tianlu Wang, Mark Yatskar, Vicente Ordonez, and Kai-Wei Chang. 2017. Men Also Like Shopping: Reducing Gender Bias Amplification using Corpus-level Constraints. In *Proceedings of the 2017 Conference on Empirical Methods in Natural Language Processing*. Association for Computational Linguistics, Copenhagen, Denmark, 2979–2989.

Table 1. Review of the coverage of [64] across different prediction tasks including both A and S . We refer to equalized odds for the anti-causal predictive case, and demographic parity for the causal predictive case, as in [72]. Here, $\{V\}$ is the set of variables to include as inputs to the model.

Predictive task	Shift	$\{V\}$
Anti-causal	demographic	$\{X\}$
	covariate	$\{A\}$
	label	\emptyset
	complex	\emptyset
Causal	demographic	$\{X, A\}$
	covariate	\emptyset
	label	\emptyset
	complex	\emptyset

APPENDIX

A RELATED WORKS AND METHODS

A.1 Fairness metrics

We define demographic parity as [4, 20, 40, 85]:

$$\max_{a \in \mathcal{A}} \mathbb{E}_{\mathbf{x}}[f(\mathbf{x}) | A = a] - \min_{a \in \mathcal{A}} \mathbb{E}_{\mathbf{x}}[f(\mathbf{x}) | A = a] \quad (1)$$

Equalized odds is computed in a similar fashion by conditioning on the positive and negative classes, taking the average of the discrepancies across classes.

Subgroup performance is computed as the accuracy (top-1 or top-3 in the case of dermatology) within each subgroup.

A.2 Causal framework

A *Bayesian network* [13, 32, 49, 50] is a *directed acyclic graph* (DAG) \mathcal{G} whose nodes X^1, \dots, X^D represent random variables and links express statistical dependencies among them. Each node X^d is associated with a *conditional probability distribution* (CPD) $p(X^d | \text{pa}(X^d))$, where $\text{pa}(X^d)$ denote the *parents* of X^d , namely the nodes with a link into X^d . The joint distribution of all nodes is given by the product of all CPDs, i.e. $p(X^1, \dots, X^D | \mathcal{G}) = \prod_{d=1}^D p(X^d | \text{pa}(X^d))$. This function is assumed to be invariant across distributions. A *path* from X_i to X_j is a sequence of linked nodes starting at X_i and ending at X_j . A path is called *directed* if the links point from preceding towards following nodes in the sequence. A node X_i is an *ancestor* of a node X_j if there exists a directed path from X_i to X_j . In this case, X_j is a *descendant* of X_i . We say that a set of nodes $\{X^i, \dots, X^j\}$ *d-separates* two random variables U and W if $U \perp\!\!\!\perp W | \{X^i, \dots, X^j\}$. A causal Bayesian network is a Bayesian network in which a link expresses causal influence rather than statistical dependence. In causal Bayesian networks, directed paths are called *causal paths*.

A.3 Feature selection mitigation strategies

We summarize the results for feature selection, and in particular the method proposed in [64] in Table 1. We observe that covariate and label shifts cannot be mitigated without excluding the signal, leading to an empty set $\{V\}$ in some of our simplified cases.

A.4 Assessing the causal structure of shifts

A.4.1 General Strategy. To assess the causal structure of a shift, we examine whether there is a direct effect of the shift S on a focal variable X^d . This requires controlling for all other pathways by which X^d may depend on S . To do this, we select a set of variables \mathbf{V} such that $\{\mathbf{V}\}$ blocks all indirect paths from S to X^d . We then test the following equality in conditional distributions: $P(X^d | \mathbf{V}, S = 0) = P(X^d | \mathbf{V}, S = 1)$ for almost all values of \mathbf{V} .⁷

To test the equality of conditional distributions, we reduce the problem to testing whether two marginal distributions of X^d are equal when the distributions of the background variables \mathbf{V} are adjusted to follow the same distribution. Using observed data from environments $S = 0$ and $S = 1$, we can perform such an apples-to-apples comparison using importance weighting. In particular, for any distribution $\pi(\mathbf{V})$,

$$P(X^d | \mathbf{V}, S = 0) = P(X^d | \mathbf{V}, S = 1) \quad \text{for almost all } \mathbf{V} \implies \quad (2)$$

$$\int E[X^d | \mathbf{V} | S = 0] \pi(\mathbf{V}) d\mathbf{V} = \int E[X^d | \mathbf{V} | S = 1] \pi(\mathbf{V}) d\mathbf{V} \implies \quad (3)$$

$$E \left[\frac{\pi(\mathbf{V})}{P(\mathbf{V} | S = 0)} E[X^d | \mathbf{V} | S = 0] | S = 0 \right] = E \left[\frac{\pi(\mathbf{V})}{P(\mathbf{V} | S = 1)} E[X^d | \mathbf{V} | S = 1] | S = 1 \right] \implies \quad (4)$$

$$E \left[\frac{\pi(\mathbf{V})}{P(\mathbf{V} | S = 0)} X^d | S = 0 \right] = E \left[\frac{\pi(\mathbf{V})}{P(\mathbf{V} | S = 1)} X^d | S = 1 \right] \quad (5)$$

Define the weights $w_0(\mathbf{V}) := \frac{\pi(\mathbf{V})}{P(\mathbf{V} | S = 0)}$, and $w_1(\mathbf{V}) := \frac{\pi(\mathbf{V})}{P(\mathbf{V} | S = 1)}$. This result shows that we can test the equality of the conditional distributions by testing the implication that the mean of weighted outcomes is the same.

This leaves a degree of freedom for choosing the test distribution $\pi(\mathbf{V})$ on which the conditional distributions will be compared. This distribution then determines the weighting scheme that will be used. We consider two different weighting schemes. In the first, we define $\pi(\mathbf{V})$ to be a constant, i.e., uniform. Then the weights are

$$w_0(\mathbf{V}) \propto P(\mathbf{V} | S = 0)^{-1} \quad \text{and} \quad w_1(\mathbf{V}) \propto P(\mathbf{V} | S = 1)^{-1}.$$

This weighting scheme is known as inverse probability weighting or IPW, and is a popular choice.

A drawback of IPW is that they can be highly variable, and inject high variance into test statistics, reducing the power of a test. An alternative weighting scheme employs so-called overlap weights (OW) [35], which correspond to the test distribution $\pi(\mathbf{V}) \propto P(\mathbf{V} | S = 0)P(\mathbf{V} | S = 1)$. This smoothly downweights values of \mathbf{V} that are rare under either $S = 0$ or $S = 1$ and focuses the comparison on values of \mathbf{V} where there is substantial overlap between the two distributions. In this case, the weights are

$$w_0(\mathbf{V}) \propto P(\mathbf{V} | S = 1) \quad \text{and} \quad w_1(\mathbf{V}) \propto P(\mathbf{V} | S = 0).$$

Note that this scheme weights each datapoint by the probability that it would appear in the opposite environment.

We estimate both OW and IPW, with a preference for OW given its favorable variance properties. We present the results with OW for compactness, and explicitly mention where OW and IPW lead to different results. It is important to note that each weighting scheme tests different implications of the equality of conditional distributions, and that falsifying either implication would indicate that the conditional distributions differ.

In practice, the likelihoods $P(\mathbf{V} | S = s)$ used to define the weights need to be learned from data. Usefully, because of how the weights are normalized, the likelihoods can be replaced with classification scores that estimate $P(S = s | \mathbf{V})$.

⁷“Almost all” specific terminology from probability theory. In most practical cases, it can be understood informally to mean “all”.

We estimate these scores with logistic regression, and plug these estimates into the expressions for our chosen weights, to obtain estimated weights \hat{w}_0 and \hat{w}_1 .

We then use a standard t-test with unequal variances to test the null hypothesis

$$H_0 : E[\hat{w}_0 X^d \mid S = 0] = E[\hat{w}_1 X^d \mid S = 1].$$

A.4.2 Testing with High-Dimensional X^d . If X^d has low dimensionality, Rabanser et al. [54] show that multiple one-dimensional tests can be used with correction for multiple comparisons (here Bonferroni). On the other hand, if X^d has higher dimensionality (e.g. an image), summaries of X^d can be constructed and the test can be performed on these lower-dimensional summaries. The validity of this approach follows from the fact that if the conditional distributions of X^d are the same, then so will the conditional distributions of any summary $f(X^d)$. The trade-off is that the test loses all power to detect distributional differences that are compressed out by the summary $f(X^d)$, or to highlight specific dimensions in X^d that are more or less affected by S . To define a summary that is relevant to the problem, Lipton et al. [36] suggest defining $f(X^d)$ to be the output of a model that predicts some variable of interest (say the outcome Y) using X^d . As reported in [54], other summarizing techniques could be considered.

B DERMATOLOGY

B.1 Assessing the shift as compound

B.1.1 The environment S affects the conditions Y . We aim at assessing the direct effect of S on Y , under the hypothesis that $P(Y|A, S = 0) = P(Y|A, S = 1)$, hence no label shift. To this end, we need to account for the effect of S on A (see causal graph in main text). Therefore, we perform overlap weighting [35] by subsampling 10,000 random samples from the source and from the target, selecting age and sex as our variables, and using the environment as our label for prediction. We train a logistic regression using 80% of the samples and assess its accuracy on the remaining 20% samples. We estimate weights for each sample in the source and in the target, normalizing the weights across samples.

For this logistic classifier, model accuracy on the left-out test sample is 66%. We note that, given the absence of ground truth, we are not able to directly assess the quality of our derived weights. Using these weights in a t-test, we obtain significant differences between the label distributions in the source and in the target for 24 conditions out of 27 ($p < 0.05$, Bonferroni corrected for multiple comparisons).

B.1.2 The environment S affects the images X . To assess the direct effect of S on the images X , we need to control for the set $\{A, Y\}$. In this case, our hypothesis is that $P(X|A, Y, S = 0) = P(X|A, Y, S = 1)$. Using a similar methodology as above, we obtain a classifier that discriminates between environments with an accuracy of 89.3%.

As X is highly multi-dimensional, we build a ‘summary’ by training a classifier that predicts the label Y from the images, following [36]. We note that we did have to train another model (without metadata compared to the model reported in the main text) to provide a summary of X , contrarily to what was reported as an advantage of the method in [36].

Based on this process, we find that 22 out of the 27 conditions (as predicted from X) lead to significant differences between the environments ($p < 0.05$, Bonferroni corrected for multiple comparisons).

B.2 Model and performance

B.2.1 Model architecture. To train the model, we consider all images pertaining to a case (min 1, max 6). Each image is encoded with a wide ResNet-101×3 feature extractor initialised using BiT-L pretraining checkpoints [31]. The

embeddings are then averaged across images and concatenated with the metadata (here age and sex) before passing through a fully connected layer which is followed by classification heads predicting the 26 + 1 conditions [37, 57]. An additional classification head covering a more fine-grained set of 419 conditions, defined on the same examples, is used at train time only.

B.2.2 Overall model performance. Detailed top-3 and top-1 model performance can be found in Tables 2 and 3, respectively. For top-1 accuracy, we observe similar results as for top-3 accuracy: model performance is relatively similar between groups on the source data, but differences become apparent on the target data (Figure 7).

Table 2. Top-3 model accuracy (in %) in the source and target data, on average across model runs.

Group	Source	Target
Total	88.52 ± 0.68	70.87 ± 0.85
Female	88.95 ± 0.93 (n=1,221)	72.11 ± 0.98 (n=10,195)
Male	87.78 ± 0.52 (n=703)	69.77 ± 0.80 (n=11,466)
[18, 30)	88.51 ± 1.11 (n=563)	87.52 ± 1.15 (n=1,434)
[30, 45)	88.38 ± 1.02 (n=548)	77.64 ± 0.79 (n=4,365)
[45, 65)	88.89 ± 0.70 (n=619)	68.39 ± 0.97 (n=8,355)
[65, 90)	87.84 ± 1.70 (n=194)	66.20 ± 1.44 (n=7,401)

Table 3. Top-1 model accuracy (in %) in the source and target data, on average across model runs.

Group	Source	Target
Total	53.62 ± 0.88	32.14 ± 0.99
Female	53.62 ± 0.88	32.34 ± 1.14
Male	55.09 ± 1.05	31.96 ± 0.91
[18, 30)	54.49 ± 1.73	45.80 ± 2.14
[30, 45)	53.12 ± 1.14	36.63 ± 1.45
[45, 65)	52.68 ± 0.92	29.32 ± 1.01
[65, 90)	55.52 ± 2.00	29.72 ± 1.05

B.2.3 Per condition model performance. We further compute model performance per condition when enough data samples are available both in the source and target data. We observe that the gaps between groups vary based on the condition, with the long tail of conditions (represented as a single ‘other’ condition in our task) showing a similar pattern as observed overall (Figure 8(a)). Some conditions like Melanocytic Nevus present disparities across age groups in both datasets (with the caveat of few test samples in the source data), with performance decreasing with increasing age (max gap in source: 24.47%, in target: 39.00%, Figure 8(b)). On the other hand, the SK/ISK condition displays similar performance across age groups in the source, but increasing performance with increasing age in the target (max gap in source: 4.00%, max gap in target: 31.78%, Figure 8(c)). Where the sample size allowed for comparisons, we therefore observe that the gaps across groups are not reproducible between the source and target data.

B.3 Second target dataset: teledermatology cases in Colombia

In this section, we repeat the analyses performed in the main text for another target dataset.

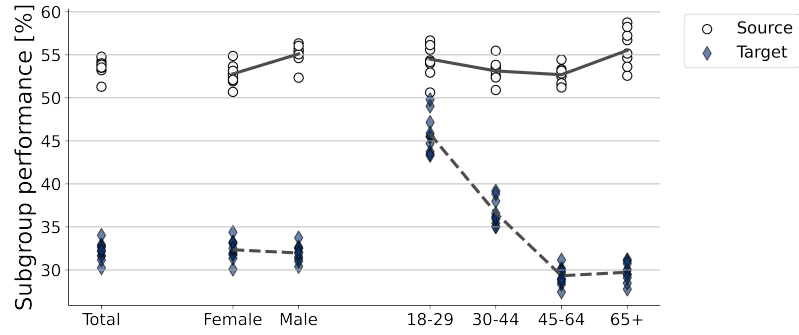


Fig. 7. Model performance in dermatology, as estimated via Top-1 accuracy (in %). The plot displays the total performance, as well as performance stratified by sex and by age on the source (circles with plain line) and target (diamonds with dashed line) data. Each marker represents one replicate of the model.

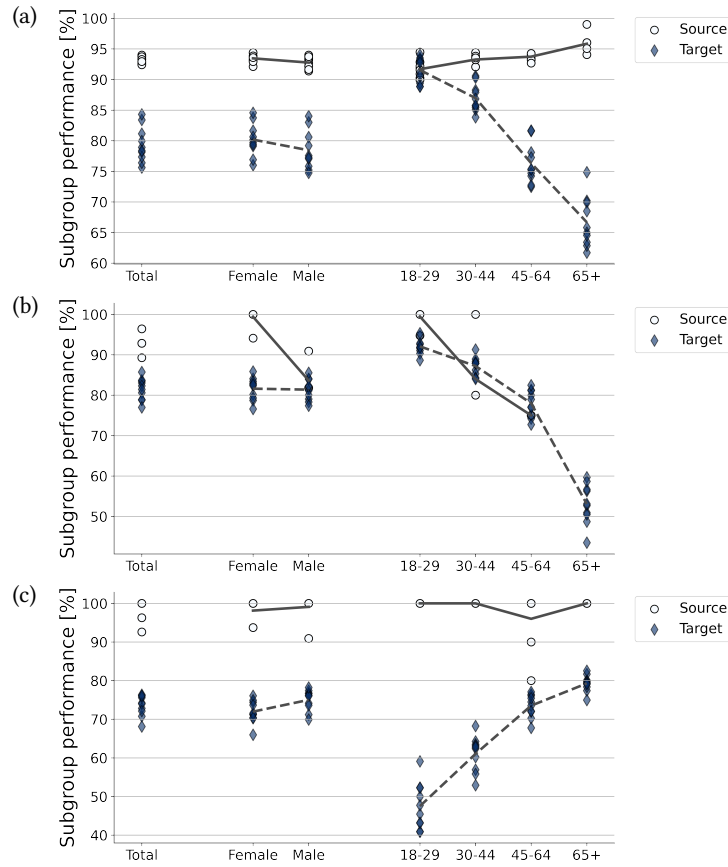


Fig. 8. Per condition model performance in dermatology, as estimated by top-3 accuracy (in %). (a) 'Other'. (b) Melanocytic Nevus. (c) SK/ISK.

B.3.1 A compound shift. As previously, we first estimate the demographic distribution of the target population (age and sex), compared to the source distribution (Figure 9(a)). We observe that the sex⁸ distributions are well matched across the source and target (binomial test, $p=0.22$). However, the target data includes a significant number of pediatric cases, and hence the age distribution is significantly affected by the shift (t-test, $p < 0.001$). We note that removing the pediatric cases still leads to a significant shift (t-test, $p < 0.001$), with the target population being on average older (median age: 44 years old, 25% quantile: 30, 75% quantile: 59) than the source population (median age: 40 years old, 25% quantile: 27, 75% quantile: 54).

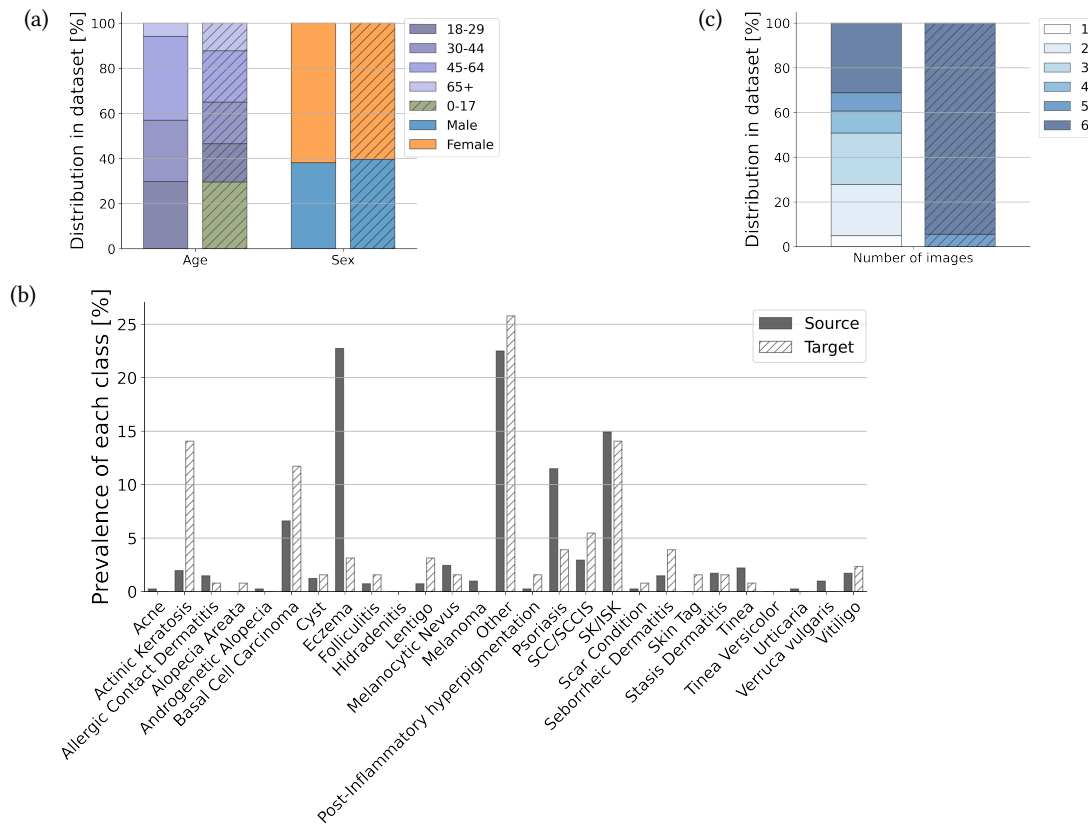


Fig. 9. Another compound shift in dermatology. (a) Distribution in each dataset of the sensitive attributes, computed in terms of percentage of pre-defined subgroups. (b) Prevalence of each condition in cases where the patients are female and over 65 years of age. (c) Distribution of the number of images in cases labelled as ‘SK/ISK’. The distributions in the source data are represented on the left, and their corresponding distributions in the target data on their immediate right with a hashed pattern.

When selecting a specific age and sex subgroup (here elder women for illustration, $n = 409$ cases in the source, $n = 128$ in the target data), we note differences in the distribution of the conditions $Y | A$ with Eczema and Psoriasis being more prevalent in the source, while conditions like Actinic Keratosis and Seborrheic Dermatitis are more represented in the target (Figure 9(b)). We note that the shift is significant for 8 conditions (i.e. $P(Y | A, S = 0) \neq P(Y | A, S = 1)$,

⁸Sex is self-reported in the target.

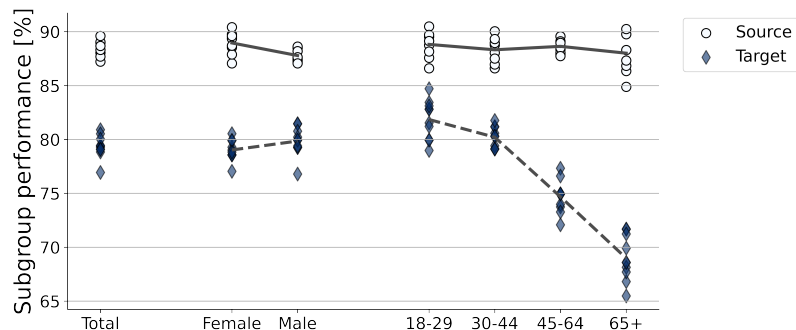


Fig. 10. Model performance in dermatology, as estimated via Top-3 accuracy (in %). The plot displays the total performance, as well as performance stratified by sex and by age on the source (circles with plain line) and target (diamonds with dashed line) data. Each marker represents one replicate of the model.

weighted t-test, $p < 0.05$ Bonferroni corrected), but is nonetheless not as stark as for the target considered in the main text.

Finally, we investigate how the images themselves are affected by S . We illustrate this difference via the number of images per case (Figure 9(c)), which displays that on average, cases from elder female patients with the ‘SK/ISK’ condition include more images in the target (median=5, $n = 18$) than in the source (median=3, $n = 61$). When assessing the hypothesis $P(X | Y, A, S = 0) = P(X | Y, A, S = 1)$ as per our weighted t-test, we observe significant differences between the source and target data for 10 conditions out of 27 ($p < 0.05$ Bonferroni corrected).

Based on these results, we observe that all aspects of the data are affected by the environment, although some conditions might display invariance (17 conditions out of 27) once controlled for demographics.

B.3.2 Fairness properties are affected by the environment. As in the main text, we then compute top-3 model performance per subgroup in the source and target distribution. We observe a similar pattern as the one depicted in the main text: while the model performs similarly across age and sex subgroups in the source dataset, performance correlates with age in the target dataset (Figure 10).

We repeat the analyses for the same conditions depicted in Section B.2.3. In this case, the tail of other conditions (‘other’, Figure 11(a)) shows more similarity with the source, and even improved performance. As previously, the fairness patterns for Melanocytic Nevus seem to be similar, decreasing with age, while SK/ISK shows an increase in performance with age in the target, but not in the source. We note that the analyses in this section include fewer samples per subgroup than in Section B.2.3 as the target dataset is smaller (1,299 adult cases in this second target compared to 21,661 cases in the target depicted in the main text).

Interestingly, using the model to predict only the 17 conditions for which we have not identified significant differences in prevalence or presentation (as per Section B.3.1) reduces the fairness gap between source and target. Figure 12 displays the model performance across those 17 conditions, where we observe a performance gap of 4.1 % in the source ($n = 412$) and 8.6 % in the target ($n = 577$). The remaining fairness gap between the source and the target could be due to interactions between age and sex, noise or unobserved variables. In comparison, using the 10 conditions for which we do have evidence of a significant shift leads to a gap of 1.1 % on the source and 10.0 % on the target. Therefore, our tests have identified potential strong drivers of the fairness gap between the source and the target environment.

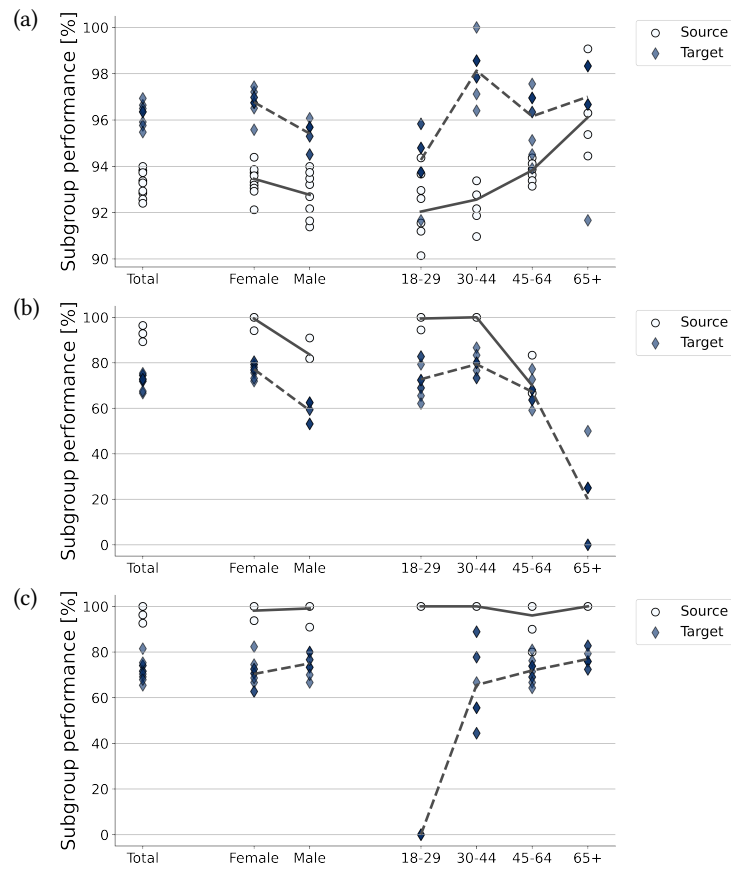


Fig. 11. Per condition model performance in dermatology, as estimated by top-3 accuracy (in %). (a) 'Other'. (b) Melanocytic Nevus. (c) SK/ISK.

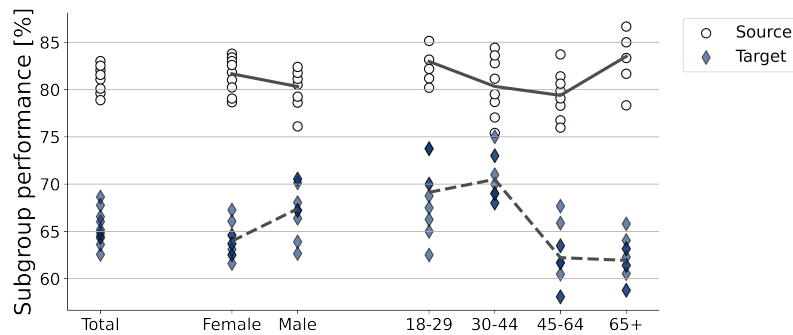


Fig. 12. Model performance in dermatology, as estimated via Top-3 accuracy (in %) for 17 conditions with $P(Y|A) \perp\!\!\!\perp S$ and $P(X|Y,A) \perp\!\!\!\perp S$. The plot displays the total performance, as well as performance stratified by sex and by age on the source (circles with plain line) and target (diamonds with dashed line) data. Each marker represents one replicate of the model.

B.3.3 Fitzpatrick’s skin type. In this second target dataset, skin type is available as an attribute. We therefore perform similar analyses as performed for age and sex. We first observe that the proportions of cases across the different skin types are different across the source and target datasets (Figure 13(a), t-test: $p < 0.001$).

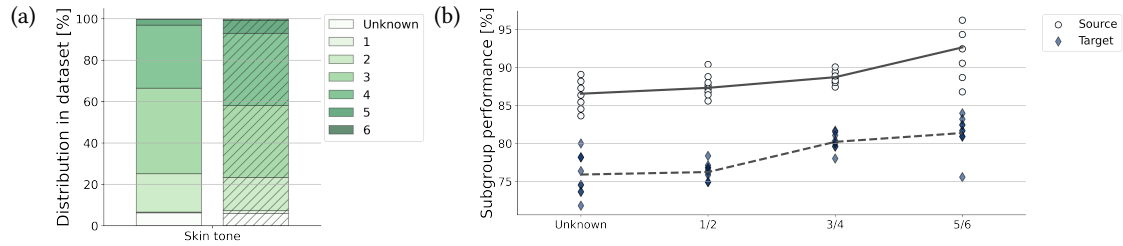


Fig. 13. (a) Prevalence of the six Fitzpatrick’s skin types in each dataset (left: source, right: target). (b) Top-3 model performance for each subgroup in the source and in the target.

Due to a low number of examples for skin types 1 and 6 (in both datasets), we group skin types according to ‘unknown’, ‘1/2’, ‘3/4’ and ‘5/6’ before assessing top-3 performance per subgroup. We observe that model performance is relatively similar across the different subgroups, with the maximum pairwise difference being 6% on the source and 5.5% on the target (Figure 13(b)). We however note that, despite the groupings, the number of examples in group 5/6 remains low (source: $n = 53$, target: $n = 131$). Performance results in this group are hence to take with a grain of salt (as displayed by large variability across seeds), and single conditions cannot be investigated.

C ELECTRONIC HEALTH RECORDS

C.1 Dataset

Cohort selection: Our cohort includes patients with age > 18 at time of admission and ICU length of stay (LOS) > 1 day. We restrict the patient sequences to the first ICU admission, as in the MIMIC-Extract project [76], and additionally restrict to only those admissions with a FIRST_CAREUNIT defined in the MIMIC-III icustays table. This procedure results in a cohort of 28,083 patients.

Feature and target definition: The full feature set from [58] is used, leading to 31,303 binary features and 28,048 numeric features. The target is defined as a binary outcome, i.e. remaining ICU LOS > 3 days, following the approach used in [52, 76].

Patient demographics are used as metadata for fairness mitigation and evaluation. For illustration, we focus on sex and age (bucketed as in the dermatology application).

Data splits: The FIRST_CAREUNIT defined in the MIMIC-III icustays table is used to split the dataset into a source dataset with 17,641 patients (MICU, SICU and TSICU) and target set with 10,442 patients (CCU, CSRU). The source dataset is then randomly split into training (80%), validation (5%), calibration (5%) and test (10%) sets.

C.2 A compound shift

C.2.1 The ICU unit S affects the comorbidities M . We define comorbidities according to [21, 71] using code in [28], obtaining a set of 30 comorbidities associated with each patient (multi-label). In this work, we refer to comorbidities as a ‘summary’ of ICD codes that represent the patient’s medical history prior to the current admission.

Statistical testing: We define OW weights based on a logistic regression that predicts the environment based on 10,000 admissions from the source and 10,000 admissions from the target data. The classifier performs with an accuracy of 59.55% on a left-out test set comprising 20% of the data. For each comorbidity, we assess whether its prevalence is significantly affected by the environment using weighted t-tests. We observe that 8 comorbidities lead to significant results (after Bonferroni correction for multiple comparisons): valvular disease, peripheral vascular, pulmonary circulation, chronic pulmonary, diabetes complicated, liver disease, solid tumor and metastatic cancer. We however caveat this analysis by the low number of patients whom have recorded comorbidities prior to admission.

C.2.2 The ICU unit S affects the treatments T . **Definition of treatments:** We identify treatments based on the ‘MedicationRequest’ field in the FHIR representation [55] of MIMIC. For each of those treatments, we construct a summary by counting the number of hourly requests in the first 24 hours after admission. This summary is used for illustrating specific medications (beta-blockers, vasopressors/inotropes and ACE inhibitors) and to control for treatments in section C.2.3. Given that this representation includes 5,873 dimensions, we build a further 1-dimensional summary [36] by training a model that predicts LOS from the time series of the medication requests on the source training split. This model reaches an accuracy of 76.9% (AUPRC: 0.54, AUROC: 0.75) on the source test split.

Statistical testing: We assess whether treatments are directly affected by S by computing weights to balance $\{A, M\}$. We note that this analysis is limited as comorbidities are not reported for all patients. Nevertheless, a binary model discriminating between environments based on $\{A, M\}$ leads to 62% accuracy. Given the dimensionality of treatments, we perform a weighted t-test on the predicted probability of the recurrent network trained to predict LOS from treatments only. Considering all medication, we observe that patients receive different treatments in different units (weighted t-test, $p < 0.0001$), hence $T \not\perp S | \{A, M\}$.

As an illustration, we estimate what proportion of patients receives treatments such as beta-blockers, vasopressors/inotropes and/or ACE inhibitors (Figure 14) for patients with (a) vascular comorbidities, and (b) tumor history.

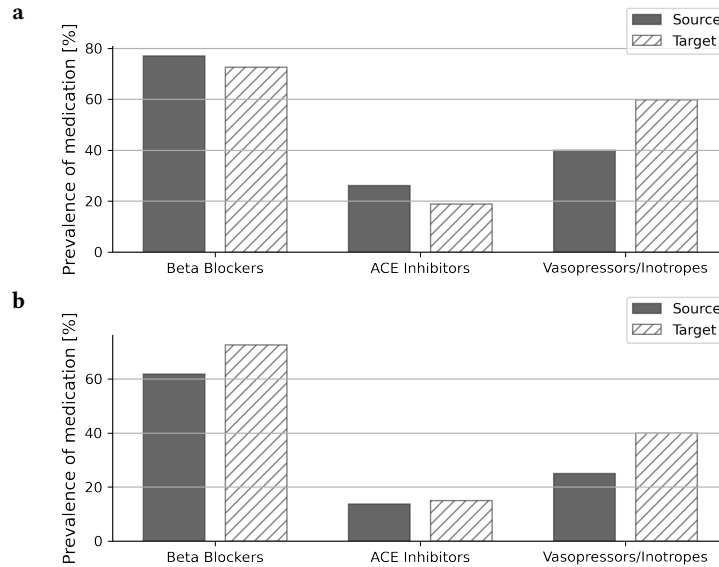


Fig. 14. Per comorbidity prevalence of treatment (in %). (a) Peripheral vascular comorbidities. (b) Solid tumor.

C.2.3 The ICU unit S affects the length of stay Y . We refer to the summary of treatments of dimension 5,873 built above to define T and build the feature set $\{A, M, T\}$ to estimate overlap weights such that we can test whether $P(Y|A, M, T, S = 0) = P(Y|A, M, T, S = 1)$. The treatment features with non-null values are normalized to be in the range $[0, 1]$ before we build a logistic regression that distinguishes between the two environments. The logistic model achieves 87.2% accuracy in predicting the environment. We derive the weights for each data point in the two environments and assess with a weighted t-test whether the prevalence in the two environments is similar. We obtain evidence that the environment directly affects the prevalence of the length of stay ($p = 0.026$ with OW, $p = 6.7e - 6$ with IPW).

Figure 15 displays the prevalence of prolonged length of stay when conditioning on specific comorbidities and treatments for older males: (a) peripheral vascular comorbidities, (b) solid tumor.

C.2.4 The ICU unit S affects the labs and vitals X . Based on the causal graph, we use the same OW and IPW weights as in Section C.2.3. We build a summary of X by predicting Y from all features that are not comorbidities, demographics or treatments. This recurrent model reaches 77.84% accuracy (AUPRC: 0.62, AUROC: 0.80) on the source test split. Based on this summary, we observe that labs and vitals display some evidence of being affected by the environment ($p = 0.011$ for OW, $p = 0.081$ for IPW). We note a discrepancy between OW and IPW results in this case.

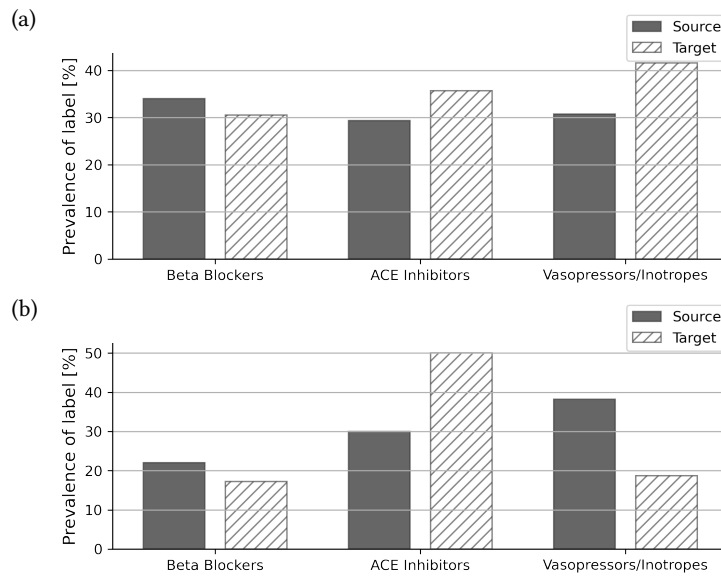


Fig. 15. Per comorbidity and treatment prevalence of prolonged length of stay (in %). (a) Peripheral vascular comorbidities. (b) Solid tumor.